UNIVERSITY OF NOVA GORICA
SCHOOL OF APPLIED SCIENCES

VACUUM ULTRAVIOLET OPERATION OF THE ELETTRA STORAGE-RING FREE ELECTRON LASER

DIPLOMA THESIS

Jurij Urbančič

Mentor: prof. dr. Giovanni De Ninno

Ajdovščina, 2009

ZAHVALA

Najprej bi se rad zahvalil svojemu mentorju prof. dr. Giovanniju De Ninnu za njegovo potrpežjivost, vodenje in podporo pri mojem delu. Rad bi se zahvalil tudi članom skupine "new light sources" iz laboratorija Elettra, še posebej Carlu Spezzaniju in Marcellu Corenu za ponujeno pomoč med mojim obiskom. Zahvaliti se želim tudi svojim staršem in starim staršem za brezpogojno podporo, ki so mi jo nudili med študijem.

ACKNOWLEDGMENT

I would like to thank my mentor prof. dr. Giovanni De Ninno for his patience, guidance and support throughout my work. His suggestions were particularly valuable. I would also like to thank the members of the "new light sources" Group at the Elettra laboratory, in particular Carlo Spezzani and Marcello Coreno who provided me with the necessary help during my visit. I want to express my gratitude to my parents and to grandparents for their unconditional support throughout my studies.

POVZETEK

To delo je bilo opravljeno v laboratoriju Elettra znotraj skupine "new light sources". Diplomska naloga je osredotočena na eksperimentalnih in numeričnih vprašanjih generiranja koherentnih harmonik na shranjevalnem obroču laserja na proste elektrone (SRFEL). Uspeli smo generirati koherentne kratke (okoli 100 fs) optične pulze v vakuumskem ultravioličnem (VUV) spektralnem območju (do 87 nm). Izvor ima stopnjo ponavljanja 1 kHz in nastavljivo polarizacijo. Namen dela je karakterizacija izvedbe delovanja izvora pri različnih valovnih dolžinah in energijah snopa elektronov. Izvedli smo tudi teoretične simulacije in primerjali dobljene rezultate z eksperimentom.

Ključne besede: laser na proste elektrone (FEL), sinhrotron, Elettra, shranjevalni obroč, ultra-relativistični snop elektronov, vakuumska ultravijolična (VUV) svetloba

SUMMARY

This work has been carried out at the Elettra laboratory within the "new light sources" Group. My thesis is focused on experimental and numerical issues about the generation of coherent harmonics on Storage-Ring Free Electron Lasers (SRFELs). We succeeded to generate coherent short (about 100 fs) optical pulses in the vacuum ultraviolet (VUV) spectral range (down to 87 nm). The source has a repetition rate of 1 kHz and adjustable polarization. The work is aimed at characterizing the source performance at different wavelengths and electron-beam energies. We also performed some theoretical studies and compared the obtained results to experiments.

Key Words: free electron laser (FEL), synchrotron, Elettra, storage-ring, ultra-relativistic electron beam, vacuum ultraviolet (VUV) radiation

Contents

LIST OF TABLES

LIST OF FIGURES

1 INTRODUCTION

The need of coherent and intense pulsed radiation is spread among many research disciplines, such as biology, nanotechnology, physics, chemistry and medicine [1]. The synchrotron light, produced by the spontaneous (incoherent[1]) emission of relativistic electrons passing through magnetic devices, only partially meets these requirements. A new kind of light source has been conceived and developed in the last decades, the result of a continuous effort of improving the performance of available light sources. This source is the Free-Electron laser (FEL).

1.1 FROM SYNCHROTRON RADIATION TO FREE ELECTRON LASERS

It is well known that a charged particle in acceleration emits electromagnetic radiation. When the energy of the particle becomes comparable to that of its rest mass, the relativistic effects induce a highly directional emission and a significant increase in the total radiated flux (the number of photons per second per unit area). Such an emission is called synchrotron radiation. Synchrotron radiation was first observed in 1947 [2] and it was initially considered as a problematic phenomenon, since it caused an undesired loss of the energy of accelerated particles. Only in the 50's it was realized that this radiation could be very useful in all scientific applications in which the structure of a particular material or sample can be studied through its interaction with light.

The first synchrotron light sources relied on accelerators built for elementary particle research, where the particles were accelerated inside the ring. In these devices, the magnetic field of bending and other magnets had to change with particle's energy. This turned out to be very demanding and also very unstable. The problem was solved with storage-rings (SR). Here the preliminary acceleration of particles is achieved by means of an external accelerator. After achieving the desired energy the particles are injected into the storage-ring, where they circulate during many hours. This improved significantly the overall stability of emitted radiation.

[1] Coherence is a property of waves that enables stationary interference.

The main disadvantage of a storage ring is that in curves the particles radiate over a large cone in the broad angle and thus only a small part of the radiation can be used for experiments. To solve this problem, the light production, initially relying on simple bending magnets (dipoles), was gradually committed to undulators, i.e. array of periodically spaced dipole magnets of alternating polarity. An illustration of the trajectory of an electron beam passing through the undulator is shown in Fig. 1.1.

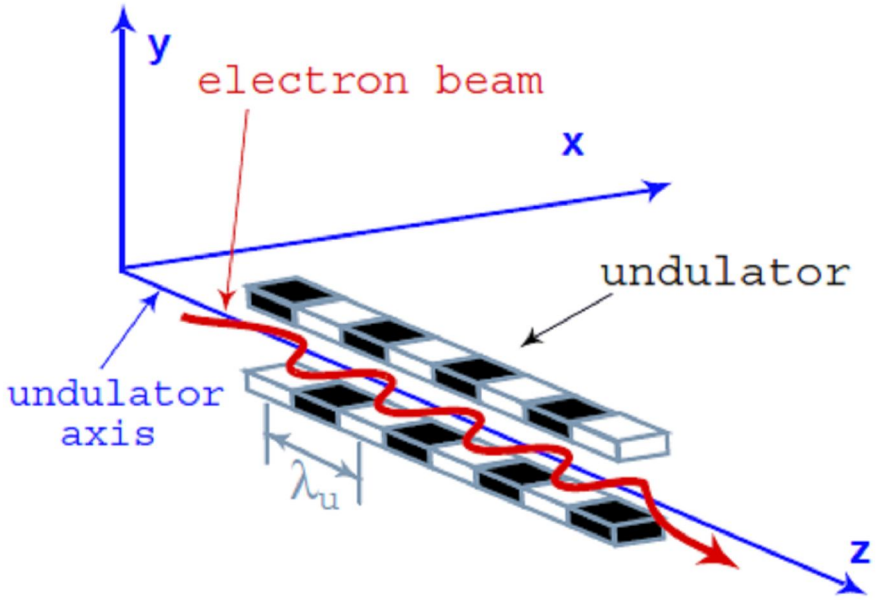

Figure 1.1: An electron beam passing through an undulator of period λ_u .

Electrons traversing the periodic magnetic structure are forced to undergo oscillations and therefore produce radiation that is much more intense and concentrated in an angle and energy spectrum significantly narrower than in the case of a simple dipole magnet. Undulators also allow us to produce radiation with different polarization (from planar to elliptical).

Today's synchrotron light sources take full advantage of undulators' feature and are designed with long dedicated straight sections to incorporate these devices. This allowed to achieve an increase in peak brightness (defined as the number of photons per pulse per unit solid angle, emitted from the unit surface of the source in a given frequency band) of around 11-12 orders of magnitude, if compared to the first synchrotrons. The evolution of synchrotron light sources in terms of peak brightness is shown in Fig. 1.2.

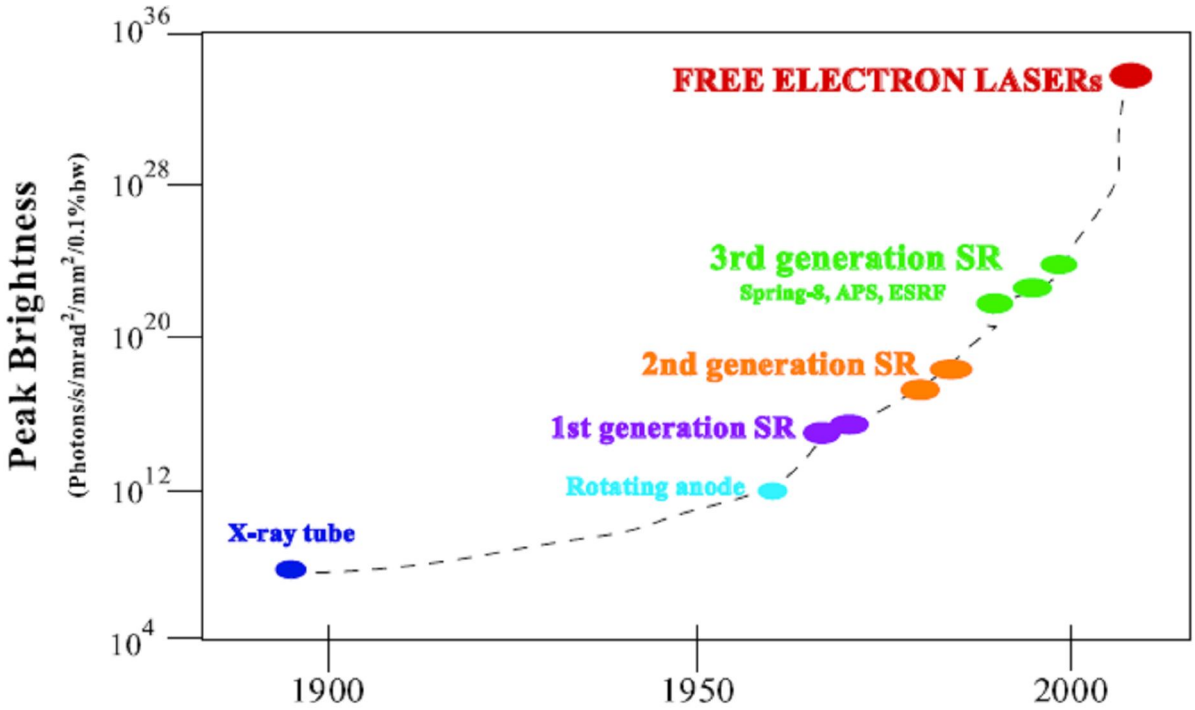

Figure 1.2: Historical evolution of peak brightness [3].

After this impressive development, the development of light sources based on the electron beams has now reached a crossroad. In fact, detailed studies have shown that the brightness of radiation from synchrotrons can not be increased significantly due to the limit reached in peak current and emittance (an explanation of the emittance will be given in Section 2.1.1).

For the next generation of UV/X-ray sources, the scientific community has oriented itself towards the development of devices that are not based on the spontaneous emission of electrons when they pass through magnetic structures, but relies instead on the interaction of the electron beam with a co-propagating electromagnetic field. Under proper conditions, the interaction between the particles and the field can result in the coherent amplification of the co-propagating wave, at both its original ("fundamental") wavelength and at its higher harmonics. A device based on this principle is called FEL. The electron beam can be provided by a linear accelerator (linac) or a storage-ring (as in the case of the Elettra FEL).

1.2 FELs: STATE OF THE ART

Two main FEL configurations can be distinguished: the single-pass configuration, where the amplification of the electromagnetic wave occurs in one passage through the undulator, and

the oscillator configuration, in which the electromagnetic wave is stored in an optical cavity and lasing is achieved as the result of a large number of light-electron interactions inside the undulator. In the following, we will concentrate on single-pass FELs.

Two different configurations can be in turn distinguished when considering single-pass FELs, depending on the origin of the electromagnetic wave which co-propagates with electrons. The first configuration, called Self Amplified Spontaneous Emission (SASE), takes origin from the spontaneous emission of the electrons propagating through the undulator. In the other case, the electromagnetic wave necessary for initiating the FEL process is provided by an external source, e.g. a conventional laser. This is the so-called seeded Harmonic Generation (HG) configuration.

In order to set a frame of reference for the experimental results presented in this thesis, the current status of the FEL sources is described here, focusing in particular on next-generation "single-pass" FELs, since this is the configuration used at Elettra.

Linac-based FELs aim at providing radiation with pulse length of about hundreds of femtoseconds in the soft and hard X-ray range. Some prototypes have been realized in the recent past in order to test both the SASE and Harmonic Generation principles. Among experiments in SASE regime, LEUTL (Low Energy Undulator Test Line) (Advanced Photon Source, Argonne, USA) has reached the 530 nm (2000) [4]; VISA (Visible to Infrared SASE Amplifier) at Accelerator Test Facility of Brookhaven National Laboratory (USA), produced FEL radiation at 840 nm (2001) [5]; TTF (Tesla Test Facility) [or FLASH (Free-electron LASer in Hamburg)] at DESY (Germany), reached the 6 nm (2007) [6]; SCSS (Spring-8 Compact SASE Source) at Spring-8 (Japan) down to 50 nm (2006) [7] and LCLS (Light Coherent Light Source) at Standford (USA) reached 0.15 nm (2009) [8]. The High Gain Harmonic Generation (HGHG) scheme has been tested at Deep Ultra Violet – FEL (National Synchrotron Light Source, BNL, USA) and reached harmonic radiation at 193 nm (2006) [9].

Most of the projects under development are based on SASE: SPARC (Frascati, Italy), 500 nm in 2009, SCSS XFEL (Spring-8, Japan) 0.1 nm in 2011, European XFEL (DESY, Germany) 0.1 nm in 2014. The only facility under construction which will be based on seeded configuration is FERMI (Trieste, Italy). This FEL will cover the range from 100 to $\leq$ 10 nm; FERMI commissioning started in summer 2009 [10].

Other proposed seeded-FELs are: Soft X-ray FEL (Berlin, Germany) with shortest wavelength: 1.2 nm, SPARX (Frascati, Italy), shortest wavelength: 1.5 nm, Arc-en-ciel (Saclay, France), shortest wavelength: 1nm. An overview of the main projects is given in Fig. 1.3.

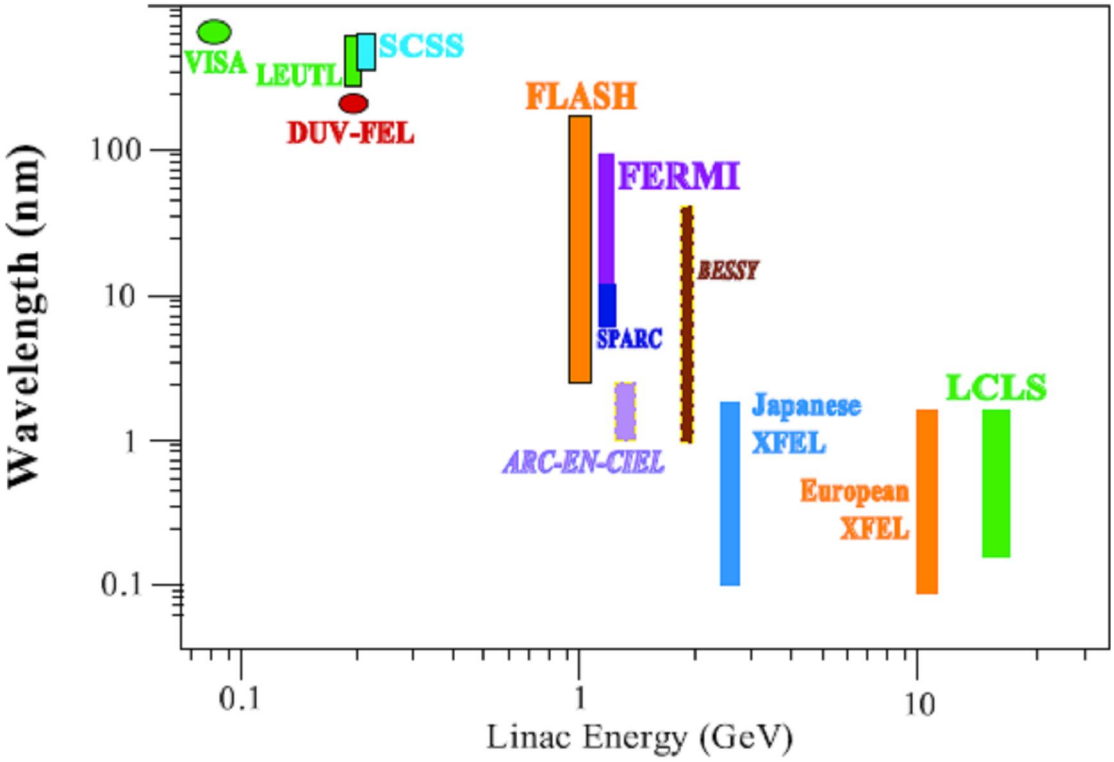

Figure 1.3: Target wavelength and linac energy of present and future FELs in single-pass configuration. SASE: VISA (USA), SCSS (Japan), FLASH (Germany), SPARC (Italy), Japanese-XFEL, European-XFEL, LCLS (USA). Seeded HG: DUV-FEL (USA), FERMI (Italy), Arc-en-ciel (France), BESSY-FEL (Germany) [11].

The improvement in terms of peak brightness of the X-FEL projects with respect to a typical 3rd generation synchrotron light source (such as Elettra) is of several orders of magnitude, as shown in Fig. 1.4. As it can be seen, FELs based on storage-rings (SRFELs) produce a radiation with intermediate brightness.

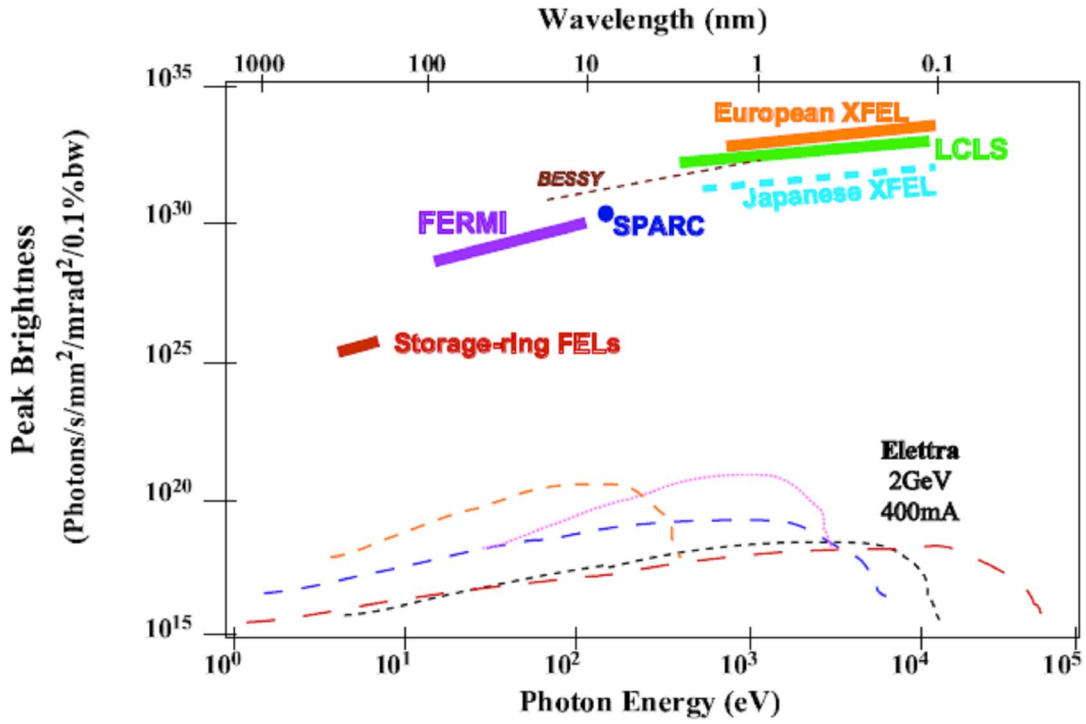

Figure 1.4: Comparison between X-FEL projects and 3rd generation synchrotron light sources in terms of peak brightness [12].

One of the key parameters of light sources is the pulse duration, which determines the temporal scale of the physical (or chemical, or biological) process that is possible to investigate. Presently, the trend is to work with pulse durations of the order of 100 fs (rms). In the near future, the aim is to reach below the femtosecond scale, approaching as much as possible the attosecond range.

The seeded single-pass configuration has been implemented only three times on storage-ring FELs. Proof of principle of generation of coherent harmonic radiation at 355 nm was first performed at LURE (Orsay, France) using a Nd:YAG laser [13]. Coherent emission at 260 nm, the third harmonic of a Ti:Sapphire laser, was observed at UVSOR (Okazaki, Japan) [14]. Recently, coherent emission at 87 nm, using also a Ti:Sapphire laser, has been reached at Elettra (Trieste, Italy) – this is the case presented in this thesis.

2 THE THEORY OF THE FREE ELECTRON LASER

Here we introduce the basic ingredients necessary for the description of the FEL process, starting from the accelerator physics.

2.1 ACCELERATOR PHYSICS

A synchrotron (also called storage ring in the following) is a particular type of cyclic accelerator: its task is not to accelerate the charged particles (normally electrons), but to maintain their energy constant for several hours. While electrons circulate, they emit electromagnetic radiation wherever they pass through bending magnets and through undulators (see Fig. 1.1). This is called "synchrotron radiation" and its production is the main objective of a synchrotron.

The electron beam is accelerated along a linear accelerator or a smaller circular synchrotron (booster) and eventually injected in a storage-ring. A storage-ring (see Fig. 2.1) is an electro-magnetic structure that consists of a series of elements providing a suitable field for bending, focusing and maintaining the average energy of the particle beam constant.

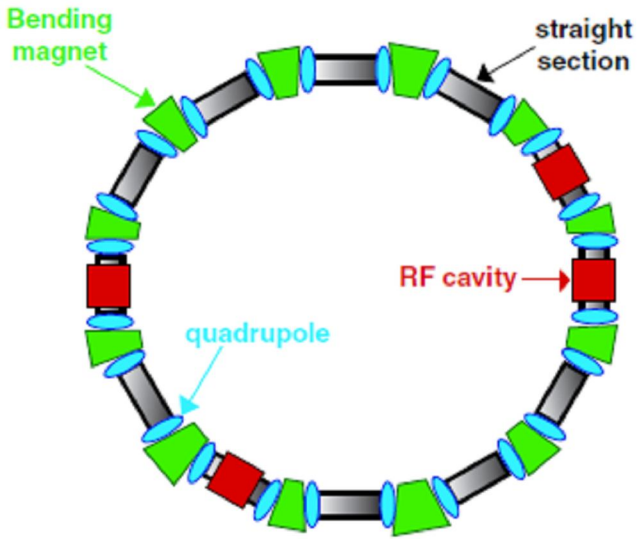

Figure 2.1: Layout of a storage-ring with main components.

The simplest possible structure consists of a "linear" lattice: it contains only those elements that provide the magnetic field for bending (dipoles), and for focusing of particles

(quadrupoles). In addition to dipoles and quadrupoles, the lattice in general also contains sextupoles and sometimes, octupoles. The role of sextupoles, which produce a magnetic field that induces non-linear components in the motion of particles, is to compensate "chromatic" effect, stabilizing the particles having slightly different energies with respect to the nominal energy of the synchrotron. The nominal energy (for which the fields produced by dipoles and quadrupoles are optimized) is such that of an ideal particle, called synchronous particle, moves on a stable closed trajectory. We will see that the motion of a generic beam particle can be described as a "deviation" with respect to the motion of the synchronous particle. The magnets that produce higher-order nonlinear components are generally used to correct multipole errors present in the fields produced by dipoles and quadrupoles [15].

The role of the radio-frequency (RF) cavities is to provide the particles with the energy they have lost due to emission during one turn around the ring. Once the radiation is produced, it is extracted and transported into various experimental chambers where it is used for different applications.

2.1.1 TRANSVERSE MOTION OF A PARTICLE BEAM

Consider the reference frame shown in Fig. 2.2.

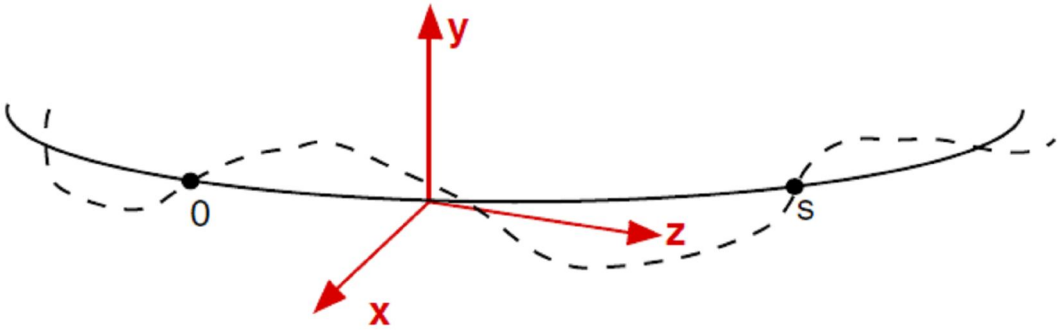

Figure 2.2: Reference frame for the electron motion in a synchrotron.

By convention the magnetic field that is produced by various magnetic elements, is set perpendicular to the direction of motion, i.e. $B_z = 0$.

Let us start considering the motion of a single particle in the transverse (x, y) plane. We define (x, p_x, y, p_y) the vector of particle coordinates in the phase space: the momenta p_x and

p_y are defined as dimensionless quantities[2] $p_x \equiv dx/dz, \;\; p_y \equiv dy/dz.$

Using the Maxwell equation

$$\nabla \cdot B = 0 \tag{2.1}$$

the magnetic field B generated by the accelerator's magnets can be written as:

$$B_y(x,y;z) + iB_x(x,y;z) = B_0\left(\rho_0 \sum_{n=1}^{\infty}\left[k_n(z) + ij_n(z)\right]\frac{(x+iy)^n}{n!} - \kappa(z)\right). \tag{2.2}$$

The function $\kappa(z)$ is equal to 1 inside the dipole and zero otherwise; B_0 is the (constant) magnetic field produced by the dipoles, necessary to maintain the ideal (synchronous) particle (with charge e and momentum p_z) in an orbit of radius ρ_0 according to the cyclotron relationship $p_z = e|\rho_0 B_0|$. The multipolar coefficients k_n and j_n, called "normal" and "skew" gradients, are defined as:

$$k_n \equiv \frac{1}{B_0\rho_0}\frac{\partial^n B_y}{\partial x^n}\bigg|_{(0,0;z)} \qquad j_n \equiv \frac{1}{B_0\rho_0}\frac{\partial^n B_x}{\partial x^n}\bigg|_{(0,0;z)}. \tag{2.3}$$

The quadrupoles generate the gradient k_1, the sextupoles the gradient k_2, the octupole k_3 etc. The skew gradients are generated from the same magnetic elements rotated by an angle of $\pi/4$ relative to the direction of propagation of the beam.

Using the development of the field given by (2.2), the equations of the particle motion in the plane (x, y) can be written as

[2] In the accelerators physics is used the longitudinal coordinate z instead of time.

$$\begin{aligned}
&\frac{d^2x}{dz^2}+\left(\frac{1}{\rho(z)^2}-k_1(z)\right)x=\mathrm{Re}\left[\sum_{n=2}^{M}\frac{k_n(z)+ij_n(z)}{n!}(x+iy)^n\right]\\
&\frac{d^2y}{dz^2}+k_1(z)y=-\mathrm{Im}\left[\sum_{n=2}^{M}\frac{k_n(z)+ij_n(z)}{n!}(x+iy)^n\right]
\end{aligned}\tag{2.4}$$

(where M represents the order of nonlinearities present in the lattice and $\rho_0(z)$ is the radius of the local curvature of the electron trajectory).

In the case of a linear lattice, i.e. $k_1\neq 0$ and $k_n=0$ for $n\neq 1$, and in the absence of the skew elements, the previous equations become the Hill equations,

$$\begin{aligned}
&\frac{d^2x}{dz^2}+\left(\frac{1}{\rho(z)^2}-k_1(z)\right)x=0,\\
&\frac{d^2y}{dz^2}+k_1(z)y=0.
\end{aligned}\tag{2.5}$$

In both directions the equations of motion are those of a harmonic oscillator, characterized by amplitude and frequency dependent on coordinate z. It is important to note that the motions in the two planes are decoupled[3]. The focusing function $k_w(z)$ (with $k_w(z)=1/\rho(z)^2-k_1(z)$ if $w\equiv x$ and $k_w(z)=k_1(z)$ if $w\equiv y$) is piecewise constant, i.e. is different from zero only inside the magnets and periodic, i.e. $k_w(z+C)=k_w(z)$, where C is the circumference of the ring.

The solution of the equations (2.5) can be written in the betatron motion form

$$w(z)=A_w\sqrt{\beta_w(z)}\cos\left[\int_0^w\frac{d\sigma}{\beta_w(\sigma)}+B_w\right],\tag{2.6}$$

where $w(z)$ represents one of the two coordinates (x or y), A_w and B_w are constants that

[3] This is true if the considered lattice does not contain magnetic elements that are skew and/or magnetic elements that produce a field along the z direction.

depend on the initial conditions and β_w is called betatron function.

The parameterization of the betatron motion is completed by the two functions

$$\alpha_w = -\frac{1}{2}\frac{d\beta_w}{dz} \tag{2.7}$$

$$\gamma_w = \frac{1+\alpha_w^2}{\beta_w}. \tag{2.8}$$

EMITTANCE

Differentiating the equation (2.6) with respect to s, we get the equation for $p_w(z)$

$$p_w(z) = -A_w\alpha_w/\sqrt{\beta_w}\cos\left(\mu_w(z)+B_w\right) - A_w/\sqrt{\beta_w}\sin\left(\mu_w(z)+B_w\right). \tag{2.9}$$

The combination of equations (2.6) and (2.9) gives the relation

$$A_w^2 = \gamma_w w^2 + 2\alpha_w w p_w + \beta_w p_w^2. \tag{2.10}$$

This equation describes an ellipse in the (w, p_w) plane. The initial condition A_w^2 represents the (constant) area of the ellipse (divided by π). The form of the ellipse and its orientation with respect to the axes (w, p_w) varies when moving longitudinally from one point of the magnetic lattice to another. The function β_w controls the form of the ellipse, α_w its orientation.

Every particle is characterized by different initial conditions and thus by a different ellipse. Most ellipses are characterized by "small" values of A_w^2: this means that the particles associated with them remain close to the origin, i.e. their motion does not differ significantly from that of a synchronous particle. Hence, the particle density will be characterized by a peak around the origin of the axes, that will decrease for larger values of A_w. Now suppose now to choose an ellipse enclosing the (e.g) 70% of beam particles and to measure the profile of the particle density along one of the two axes: this is equivalent to projecting the population of particles in phase space along the considered direction. This profile is generally characterized by an approximately Gaussian shape. The standard deviation of this profile

(σ_w) is the parameter that is normally used to indicate the size of the beam and to define its geometric emittance ε_w:

$$\varepsilon_w = \frac{\pi\sigma_w^2}{\beta_w}. \tag{2.11}$$

Thus, the geometric emittance is defined as the area of the ellipse in the phase plane (w, p_w) whose maximum amplitude along the coordinate z is σ_w, or also as the area of ellipse that contains about 70% of the beam particles. The geometric emittance is an invariant of the motion only if: a) the beam is not accelerated and b) we can neglect the "dissipative" effects due to particle energy loss by radiation (synchrotron radiation). In a first approximation the latter is true only if the particles circulating in the ring are "heavy" (such as protons). In case of protons, if the beam is accelerated, the geometric emittance decreases proportionally to the inverse of the beam energy.

To obtain a parameter representing the area of the beam in its phase space that is invariant even when the protons are accelerated, one needs to multiply the geometric emittance by the product $\beta\gamma\left(\beta = v/c\right)$. The normalized emittance $\varepsilon_{n,w}$ is defined as:

$$\varepsilon_{n,w} = \beta\gamma\varepsilon_w. \tag{2.12}$$

$\varepsilon_{n,w}$ is a constant of motion even in presence of acceleration (neglecting the dissipative effects).

In case where the particles circulating in the ring are "light" (such as electrons), the dissipative effects due to synchrotron emission can not be neglected and the system can no longer be considered as conservative. In this case, the equilibrium conditions of the beam (both longitudinal and transverse) are the result of two phenomena that compete with each other: the energy loss due to synchrotron emission, which tends to collapse the beam size, and the excitation due to the fact that electrons emit photons stochastically (according to quantum mechanics), tending to increase the size of electron distribution. In this case the geometric emittance at equilibrium varies (approximately) with the square of the beam energy.

2.1.2 LONGITUDINAL MOTION

A charged particle e that is moving with a velocity v in a region with an electromagnetic field is subject to the Lorentz force $\vec{F}$

$$\vec{F} = e\vec{E} + e\left(\vec{v} \times \vec{B}\right). \tag{2.13}$$

where $\vec{E}$ is the electric field, e is the electric charge of the particle, $\vec{v}$ is the instantaneous velocity of the particle and B is the magnetic field.

Because the term $e\left(v \times B\right)$ is perpendicular to the trajectory and does not do work, the only way to provide energy to the particle is via an electric field. This is the task of the RF cavity (see Fig. 2.1), a device that provides an electric field that is parallel to the trajectory of the particle. The generated electric field is sinusoidal and is characterized by a frequency ω_{rf},

$$\vec{E_z}(t) = \vec{E}_0 \sin(\omega_{rf} t + \psi_0). \tag{2.14}$$

(ψ_0 is a phase constant). The value of ω_{rf} is chosen so that it is a harmonic number h of the revolution frequency ω_r of particles in the ring,

$$\omega_{rf} = h\omega_r; \tag{2.15}$$

h is called the harmonic number. The energy gain of a generic particle in a bunch in one revolution is

$$\left(\Delta E\right)_{turn} = e\hat{V} \sin\phi(t) \tag{2.16}$$

where $\hat{V}$ is the peak of the potential difference that the particle finds at the passage through the cavity and $\phi(t)$ is the phase value of the field seen by the particle.

In the case of a synchrotron, the energy gain $(\Delta E)_{turn}$ compensates exactly the energy lost in one turn from the synchronous (ideal) particle due to synchrotron radiation. This energy is

$$(\delta E)_{\sin} = 88.4 \frac{E^4[\mathrm{GeV}]}{\rho[\mathrm{m}]}. \tag{2.17}$$

The synchronous particle circulates on a trajectory that goes through the center of all magnets and is therefore characterized by a betatron oscillation that is equal to zero. When this particle is passing through the cavity, it always finds the same phase of the field:

$$\phi(t) = \phi_z. \tag{2.18}$$

We now distinguish two cases: one relevant to the acceleration and/or the "storage" of "heavy" particles, and one relevant to the "storage" of "light" particles. In the first case we consider the energy lost due to synchrotron emission as negligible. We will then see how the results change when dissipative effects associated with the synchrotron emission are considered.

THE CASE OF HEAVY PARTICLES

As in the case of transverse dynamics, the longitudinal motion of a generic beam particle is characterized as a deviation from that of the synchronous particle. It is possible to demonstrate that the motion of the generic particle is governed by the following equations

$$\begin{aligned} \frac{dW}{dt} &= e\hat{V}\left(\sin\phi - \sin\phi_z\right), \\ \frac{d\phi}{dt} &= -\frac{1}{2\pi}\frac{h\eta\omega_z}{p_z R}W, \end{aligned} \tag{2.19}$$

where $\phi = \phi_z + \Delta\phi$ is the phase of the particle, p_z and ω_z represent the momentum and the revolution frequency of a synchronous particle, $\eta = \frac{d\omega}{\omega_z} / \frac{dp}{p_z}$ and $W = 2\pi R \Delta p$. The variables ϕ and W are canonically conjugated: (ϕ, W) represents the phase plane relative to the longitudinal motion. If the parameters R, p_z, η, ω_z, $\hat{V}$ vary slowly in time with respect to

$\Delta\phi$, the equation for the phase becomes

$$\ddot{\phi} + \frac{\Omega_z^2}{\cos\phi_z}\left(\sin\phi - \sin\phi_z\right) = 0 \tag{2.20}$$

where

$$\Omega_z = \sqrt{\frac{e\hat{V}h\eta\omega_z\cos\phi_z}{2\pi Rp_z}} \tag{2.21}$$

is called the frequency of the synchrotron. For $\Delta\phi \ll 1$ (small oscillations) the equation of motion assumes the form

$$\ddot{\phi} + \Omega_z^2\Delta\phi = 0. \tag{2.23}$$

According to equations (2.21) and (2.22), when the product $\eta\cos\phi_z$ is positive, the motion with small amplitude around the synchronous phase is the harmonic oscillator motion (i.e. a circle in the phase plane (ϕ, W)). The parameter η is $\frac{1}{\gamma^2} - \alpha$, where γ is the nominal normalized energy of the electron beam and $\alpha = \frac{dL}{L} / \frac{dp}{p_z}$ is called the "momentum compaction" and is a constant parameter combining the variation of the orbit length L of a given particle with the corresponding momentum variation. Usually α is positive. The parameter η becomes negative when $\gamma > \gamma_{tr}$, where $\gamma_{tr} = \sqrt{1/\alpha}$ is called the "transition energy". According to (2.21), the oscillations of the synchrotron are stable when $\eta > 0$ and $0 < \phi_z < \pi/2$, or $\eta < 0$ and $0 < \phi_z < \pi$ (principle of phase stability). When, during the acceleration, γ becomes equal to γ_{tr}, the phase of the radiofrequency has to be rapidly moved from ϕ_z to $\pi - \phi_z$, otherwise the beam becomes unstable.

Back to equation (2.20), multiplying both sides by $\dot{\phi}$ and integrating we obtain the following invariant of motion

$$\frac{\dot{\phi}^2}{2} - \frac{\Omega_z^2}{\cos\phi_z}\left(\cos\phi + \phi\sin\phi_z\right) = \text{cost.} \tag{2.23}$$

Relaxing the condition of small fluctuations around the energy and phase of the synchronous particle, the circles in the phase space are distorted by nonlinear motion (according to equations (2.19)). Trajectories in phase space continue to close in on themselves until ϕ reaches the critical value $\pi - \phi_z$. For this value the factor $\sin\phi - \sin\phi_z$ in the equation of motion (2.20) becomes zero and for larger values ϕ the force becomes repulsive and the motion unstable. The curve that corresponds to $\phi = \pi - \phi_s$ is called separatrix and satisfies the equation

$$\frac{\dot{\phi}^2}{2} - \frac{\Omega_z^2}{\cos\phi_z}\left(\cos\phi + \phi\sin\phi_z\right) = -\frac{\Omega_z^2}{\cos\phi_z}\left(\cos\left(\pi - \phi_z\right) + \left(\pi - \phi_z\right)\sin\phi_z\right). \tag{2.24}$$

In practice, according to the relationship (2.15), the radio-frequency field makes a number h of oscillations during one period of revolution of the particles. This means there are h synchronous particles around which a dynamic governed by equation. (2.19) is developed. The beam is divided into h packets, typically a few centimeters long.

THE CASE OF LIGHT PARTICLES

As said before, in the case of the synchrotron the energy gain from the RF cavity serves to compensate (exactly) the energy loss of the synchronous particle in one passage through the bending magnets (i.e. dipoles and undulators). The dynamics of other particles, characterized by a different phase and energy with respect to the synchronous particle, can be described by the equation of motion (2.19) including the dissipative effects associated with the synchrotron emission. The differential equation for the energy loss $\Delta E\left(\propto W\right)$ in case of small oscillations takes the form

$$\frac{d^2}{dt^2}\Delta E + 2\alpha_d \frac{d}{dt}\Delta E + \Omega_z^2 \Delta E = 0. \tag{2.25}$$

The solution has a form of a damped oscillator,

$$\Delta E = A\exp\left[-\alpha_d t\right]\cos\left(\Omega_z t + B\right) \tag{2.26}$$

(with constant A and B). Under suitable approximations it can be shown that the time of damping of the oscillations is

$$\tau_d = 1/\alpha_d = T_0 E/\left(\delta E\right)_{sin} \tag{2.27}$$

(where T_0 is the revolution period of the particles inside the ring and $\left(\delta E\right)_{sin}$ is given from (2.17)): τ_d can be interpreted as the time required to radiate an energy that is equivalent to the total energy of the particles. According to equation (2.26), the synchrotron oscillations damp down and the particle beam tends to collapse (in phase and energy) on the synchronous particle. In reality, this damping is opposed by several phenomena. First, the emission of photons from the particles occurs in discrete quanta. This induces an increase of emittance (longitudinal and transverse) and imposes a lower limit to the collapse of the size of the beam. Another limitation is due to the scattering between the particles, an effect that becomes more important as the beam becomes denser. Other mechanisms that oppose the damping of synchrotron oscillations are, for example, the scattering with the residual gas in the vacuum chamber where the particles are circulating, and inevitable fluctuations of the RF voltage. The final size of the beam results from the equilibrium between the damping of synchrotron oscillations and the mechanisms of excitation.

2.2 FEL PRINCIPLE

The basic principle of the FEL emission relies on the interaction between a relativistic electron beam and a co-propagating electromagnetic wave in the presence of a static and periodic magnetic field, provided by an undulator. The undulating electrons radiate energy mainly within a cone in the direction of motion. The electrons radiate at a wavelengths λ_s determined by the resonance condition [16]

$$\lambda_s = \frac{\lambda_u}{2\gamma^2}\left(1 + K^2 + \gamma^2\theta^2\right). \tag{2.28}$$

Here K represents the strength of the undulator and is proportional to the on-axis peak and to the magnetic period of the undulator λ_u, θ is the emission angle measured with respect to the undulation axis and γ is the normalized electron beam energy. The resonance condition allows selecting of the suitable resonant wavelength for the undulators.

If the electron beam could be represented by a homogeneous moving charged fluid, no net radiation in an undulator would be produced. In fact, for each radiating slice of the beam, the corresponding slice at $\lambda_s / 2$ longitudinal separation radiates at the opposite phase and cancels the radiation of the first slice. In practice a beam is granular and the radiated power is proportional to the number of electrons N_e. When all electrons radiate in phase, not the net power but the amplitude of the radiation is proportional to N_e. As a consequence, the resulting output power is proportional to N_e^2. In order to get coherent radiation and reach much higher amplitude, micro-bunching is thus needed because only radiation from the electrons spaced at one or more wavelengths interferes constructively (in a continuous beam we also get destructive interference by out of phase particles). This micro-bunching is induced by the force exerted by the light on the electrons.

2.2.1 SINGLE-PASS CONFIGURATION

The main reason for the great interest in developing single-pass FELs that do not need mirrors to store the electromagnetic wave in an optical cavity is the lack of robust materials with high reflectivity in the VUV and X-ray range. Another reason is the great progress in performance of competitive conventional lasers that are cheaper than the FEL oscillators. In single-pass configuration, the electron beam interacts with the electromagnetic field and amplifies it in a single pass through the undulator. The single-pass configuration is usually implemented on a linear accelerator (linac). Rarely is it implemented on a storage-ring such as Elettra.

In the SASE configuration (see Fig. 2.3) a linear accelerator provides the electrons that pass through a long (tens of meters) chain of undulators. The spontaneous emission produced by electrons at the entrance of the undulator is coupled to the beam and gets amplified. SASE sources are relatively simple to implement and are characterized by very high brightness. However, since SASE originates from spontaneous emission, it is quite “noisy”: the emitted

radiation consists of a series of spikes with variable duration and intensity.

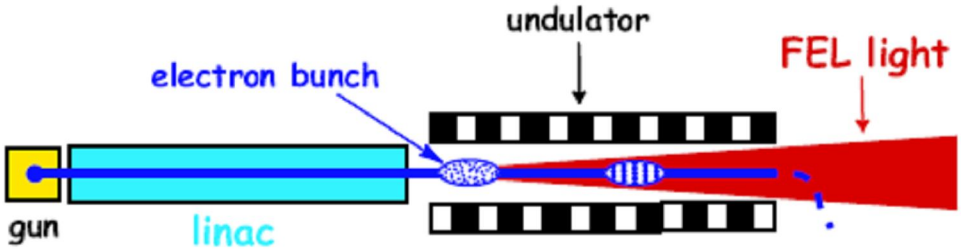

Figure 2.3: SASE FEL in single-pass configuration.

The electromagnetic wavelength amplified by the electrons is given by the resonance condition in Eq. 2.28. The light characteristics strongly depend on electron beam properties. For example, if different bunches have significantly different currents the radiation will also display significant shot-to-shot fluctuations on the intensity or on the wavelength, respectively. The SASE output has very good spatial mode and is easily tunable by varying the energy of the electrons and/or the undulator parameter K.

The other configuration is obtained when the electromagnetic wave necessary for the FEL process is provided by an external light source (generally a conventional laser). From now on, we will concentrate on this configuration, since this is the configuration used at Elettra. In this case, the generation of coherent harmonics is based on the up-frequency conversion of the (high) laser power through the interaction with the relativistic electron beam. The working principle of a seeded FEL will be explained more in detail in the following section.

2.2.2 BUNCHING

When an electron beam starts to interact with an electromagnetic wave the phase of all the particles is randomly distributed with respect to the wave, as shown in Fig. 2.4a.

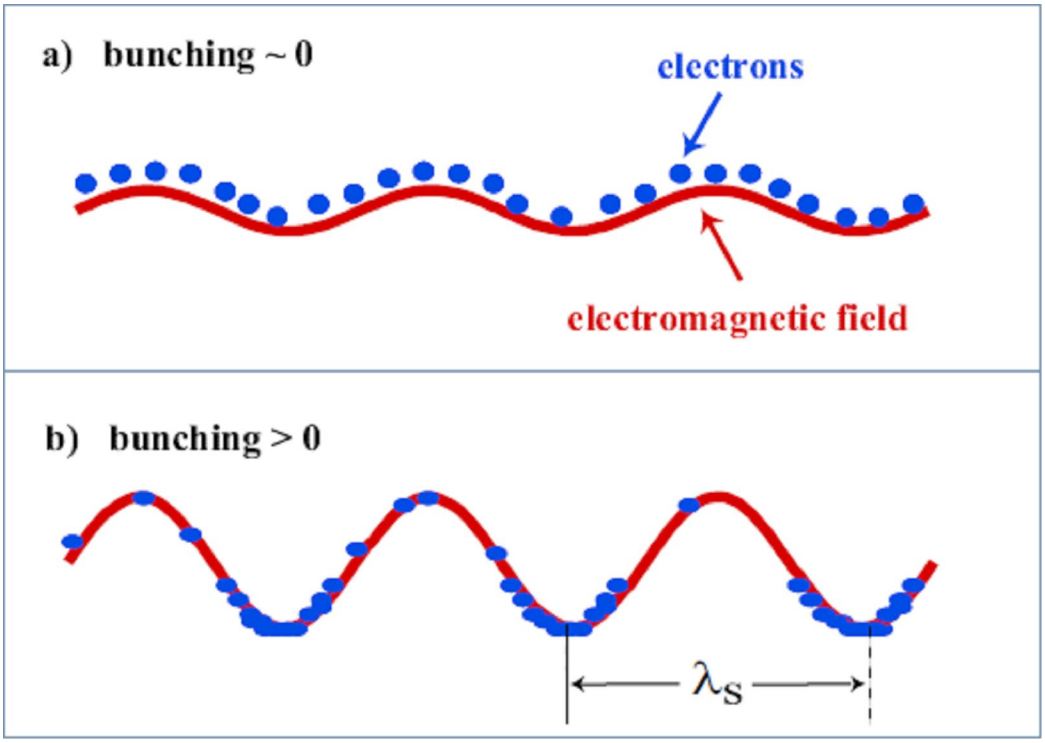

Figure 2.4: Bunching evolution. (a) Electrons are randomly distributed in phase (initial condition). (b) Electrons start bunching on a λ_s scale and the wave is eventually amplified.

As the resonance condition is satisfied, i.e. the velocity of the electrons is equal to the phase velocity of the radiation + undulator field (ponderomotive field), half of the particles absorb energy from the electromagnetic wave and the other half transfer energy to the wave. Therefore the amplification is zero.

The interaction with the ponderomotive wave induces a modulation of the electron energy. This energy modulation evolves in spatial modulation, also called bunching. As the beam proceeds further inside the undulator, the spatial modulation arises also where the ponderomotive force is positive and this causes "over-bunching". Here the process reaches the saturation because the electrons are not able to transfer their energy to the wave anymore. The saturation is not a stationary state since the system does not arrive at an equilibrium condition. Fig. 2.5 explains the saturation mechanism, as it occurs in the electron phase space (γ, θ).

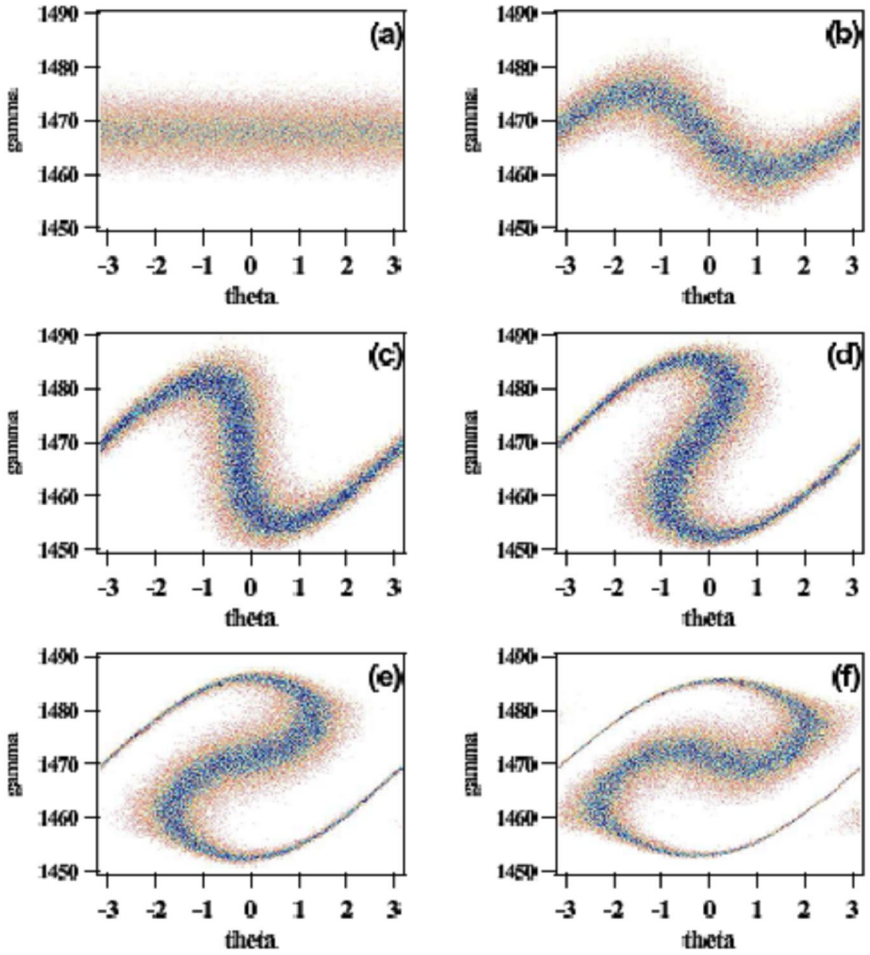

Figure 2.5: Evolution of the electron-beam phase space. (a) Initial distribution, (b) energy modulation, (c) spatial modulation (bunching), (d) slight overbunching (e-f) overbunching [11].

The evolution of the spatial separation of the electrons at the scale of the resonant wavelength is schematically shown in Fig. 2.6.

Figure 2.6: The evolution of the spatial separation (bunching) in an electron bunch [11].

2.2.3 HARMONIC GENERATION

In the single pass case, the usual configuration for harmonic generation (HG) relies on the seeding technique (i.e., the use of an external laser) and makes use of two undulators: the first undulator is tuned to the same wavelength as the external laser and the second one is tuned to the selected harmonic. Between the two undulators there is a dispersive section, which has the role to help the conversion of the energy modulation into bunching. A schematic picture of the scheme under investigation is shown in Fig. 2.7.

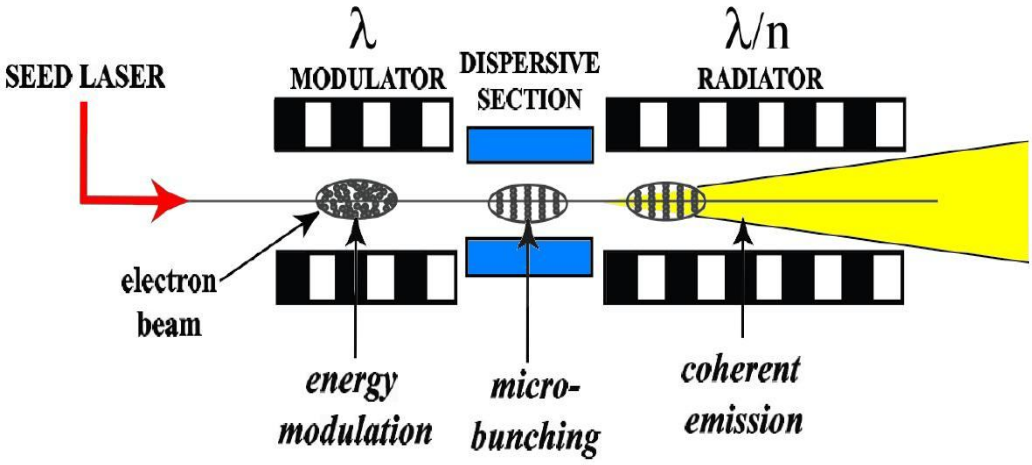

Figure 2.7: Seeded Harmonic Generation scheme.

In the first undulator the interaction between the seed laser and the electron beam produces a modulation in the energy distribution of electrons at the wavelength of the external laser. At the beginning (Fig. 2.8a), the electron-beam energy distribution has a random phase with respect to the electromagnetic field provided by the seed laser and is characterized by an initial (incoherent) energy spread. During the interaction with the seed, some electrons lose and some electrons gain kinetic energy. As a consequence, the energy distribution is clearly modified, as shown in Fig. 2.8b. The magnetic field of the dispersive section forces the electrons with different energies to follow different paths. Therefore, the passage through the dispersive section converts the energy modulation in spatial bunching. The corresponding phase space is shown in Fig 2.8c. Finally, in the second undulator that is tuned to one of the harmonics of the seed laser, the electrons produce coherent light since each "micro-bunch" emits radiation as a macro-particle.

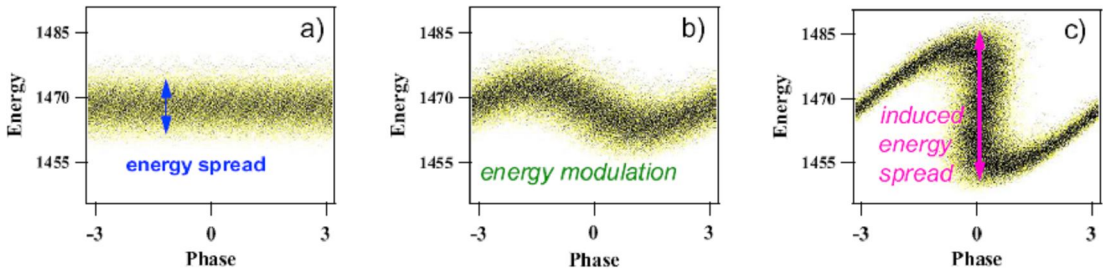

Figure 2.8: Phase space (γ, θ) evolution. (a) Initial distribution, (b) energy modulation and (c) micro-bunching [11].

If the electron beam is flat in current and energy, i.e. no quadratic (or higher order) chirp in the two energy distributions, the spectrum of the extracted radiation is expected to be close to the transform limit.

As the electron beam has a pulsed structure, the seed pulse has to be synchronized with the electron bunch. The pulse duration at the exit of the radiator is determined by the duration of the seed pulse.

3 EXPERIMENTAL SETUP

The experimental setup for the coherent harmonic generation (CHG) at Elettra is based on the SRFEL equipment. A Ti:Sapphire laser provides the seed for harmonic generation. The interaction with the seed laser (and the consequent emission) occurs in a single pass, as in a linear accelerator, but in this case the electron beam is re-circulated. This means that the electron-beam properties, notably the mean energy and the peak current, are "thermalized" by a long-lasting periodic dynamics. This in principle results in a very good reproducibility of the seeding process and, as a consequence, in an excellent shot-to-shot stability of the optical pulse produced at the end of the device. On the contrary, in the case of a single-pass linac-based FEL, successive electron bunches delivered by a linac are generally characterized by significant fluctuations of the mean electron-beam energy and current. In general, this may result in a conspicuous shot-to-shot instability of the emitted harmonic power. In the following, we describe the experimental setup of the Elettra SRFEL. We will also report on some important issues concerning the temporal (longitudinal) and transversal alignments of the laser and electron beams.

3.1 THE OPTICAL KLYSTRON

The experimental setup for CHG at Elettra is based on the optical klystron (OK) installed on the storage ring. This device has been built and used for a long time only for the SRFEL in oscillator configuration (see Fig. 3.1).

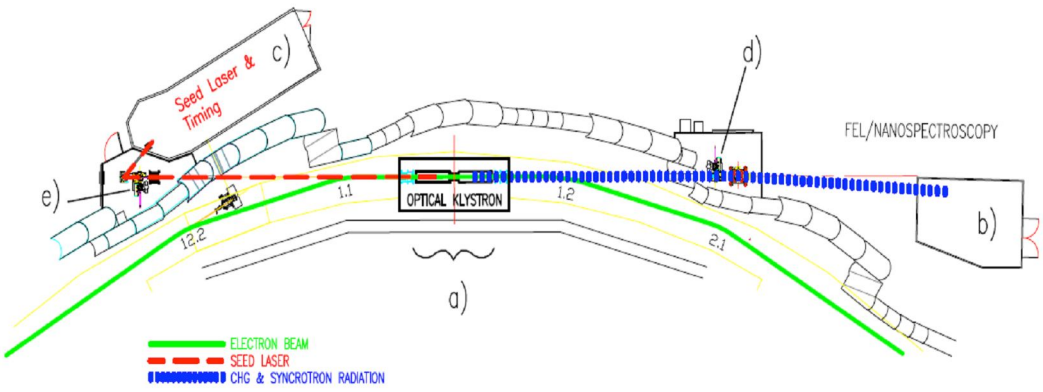

Figure 3.1: Layout of the Elettra section 1 where the optical klystron for the FEL beamline is installed. (a) FEL optical klystron. (b) Front-end station. (c) Laser hutch and back-end station. (d) Mirror chamber.

The general layout of the Elettra FEL beamline is shown in Fig. 3.1 The optical klystron consists of two APPLE-II type permanent magnet undulators, one called modulator (ID1) and one the radiator (ID2), together with a three-pole electro-magnet called the dispersive section (DS). Both the gap and the phase of the APPLE-II undulators can be tuned independently. Each undulator can be tuned to different wavelengths and the polarization can be varied continuously from linear to elliptical. The dispersive section is a three-pole electro-magnet allowing continuous variation of the R_{56} parameter from 0 to 70 μm. Table 3.1 summarizes the main parameters of the optical klystron.

Table 3.1: The relevant parameters for the Elettra OK [17].

Undulators: ID1 and ID2	
Type	APPLE II permanent magnet
Period	100 mm
Number of periods	20
Minimum gap	19 mm
λ 1st harm. (gap = 19 mm, phase = 0)	756 nm at 0.9 GeV 272 nm at 1.5 GeV 153 nm at 2.0 GeV
Dispersive section: DS	
Type	Electromagnetic 3-pole
Length	50 cm
Maximum field	0.8 T

To maximize the coupling between the electromagnetic field and the electron bunch inside the modulator, the seed polarization must be the same as the polarization at which ID1 is set. ID2 can be set either for linear or circular polarization. This determines the polarization of the coherent emission. The DS strength is varied to optimize the micro-bunching of the electron beam.

The optical klystron was designed both to be compatible with normal operations of the

beamline at high electron energy and to provide light in the visible-VUV range for the FEL operations at low electron energy.

3.2 ELETTRA STORAGE RING

Elettra is an SR dedicated to the production of synchrotron radiation and is usually operated in multi-bunch mode. It was designed to work at electron beam energies in the range 1.5-2.0 GeV. Nowadays, to satisfy the user-community requests, Elettra is usually operated at 2.9 or 2.4 GeV, improving the beam lifetime and shifting to higher energies the photon emission spectrum from bending magnets and insertion devices. As can be seen from Table 3.1, since the modulator must be tuned to the wavelength of the seed laser ($\lambda \geq 260$ nm, see the next paragraph), the limitation on the minimum undulator gap, restrict the values for a suitable beam energy for CHG to the range 0.75-1.5 GeV. This consideration represents the main limitation to the compatibility of CHG experiments with standard user operation, and makes necessary to allocate dedicated machine shifts for this activity.

When a seeded CHG experiment is performed, the potential beam instabilities that can limit or prevent the light amplification have to be taken into account. As the output power of the CHG process depends quadratically on the number of electrons interacting with the seed multiplied by the bunching factor – the later being proportional to the laser power – any fluctuation of the overlap between the electron beam and the laser will result in significant deterioration of the output power stability. Electron beam instabilities are particularly harmful when Elettra is operated below 0.9 GeV, because at those energies the magnets' power supplies are forced to work far from their standard range. As a consequence, they provide unstable guiding fields that perturb the electron beam dynamics.
There are four RF cavities to supply the energy lost by synchrotron radiation to electrons. The cavities operate at 500 MHz. The summed voltage of cavities determines the longitudinal energy acceptance of the machine.

In one of the 12 straight sections an optical klystron is accommodated that can act either as a standard synchrotron light source or as the interaction region for the FEL.

Table 3.2: Elettra parameters for SRFEL operation [17].

Electron beam energy	0.75 – 1.5 GeV
Ring circumference	259.2 m
Orbit period	864 ns
Orbit frequency	1.157 MHz
RF frequency	499.654 MHz
Harmonic number	432
Momentum compaction factor	0.00161
β_x at ID center	8.2
β_y at ID center	2.6
Normalized x-emittance (1 GeV)	3.2 mm mrad
Normalized y-emittance (1 GeV)	0.2 mm mrad
Number of bunches	1 – 4
Max current per bunch	6 mA
Natural (i.e. low-current) RMS energy spread	0.12% at 0.9 GeV 0.23% at 0.75 GeV 0.08% at 1.5 GeV
Natural (i.e. low-current) RMS bunch-length	5.4 ps at 0.9 GeV 4.1 ps at 0.75 GeV 11.6 ps at 1.5 GeV
RMS energy spread at 6 mA	0.036% at 0.9 GeV 0.030% at 0.75 GeV 0.060% at 1.5 GeV
RMS bunch-length at 6mA	27 ps at 0.9 GeV 28 ps at 0.75 GeV 25 ps at 1.5 GeV
Peak current at 6 mA (0.9 GeV)	~ 80 A
ε_x (0.9 GeV)	~ 1.4 mm μrad
ε_y (0.9 GeV)	~ 0.14 mm μrad
σ_x (0.9 GeV)	1.1×10^{-4} m
σ_y (0.9 GeV)	2.6×10^{-5} m

3.3 THE SEED LASER

The seed laser is a multi-stage system including an IR oscillator developed for the laser group in Elettra and a Legend amplifier assembled by Coherent [18]. The oscillator is a passive model locked Ti:Sapphire cavity pumped by a 4.5 mW diode laser. The mode locking allows entering in a pulse regime that is adapted to the total cavity length. Such a length has been chosen in order for the repetition rate of the laser to be commensurate with the repetition rate of the synchrotron. This allows the synchronization. When optimized, the oscillator delivers 120 fs (FWHN) pulses with 3 nJ energy per pulse at the fundamental wavelength in the range 780-800 nm. The oscillator emission seeds the Legend amplifier which increases the energy of a single pulse up to 2.5 mJ at the fundamental wavelength. The pulse duration can be changed by means of two compressors with a flipper that allows switching. In particular, two different schemes can be chosen in order to obtain either 100 fs or 1 ps "transform limited" pulse. The operational repetition rate range is between 1 Hz to 1 kHz.

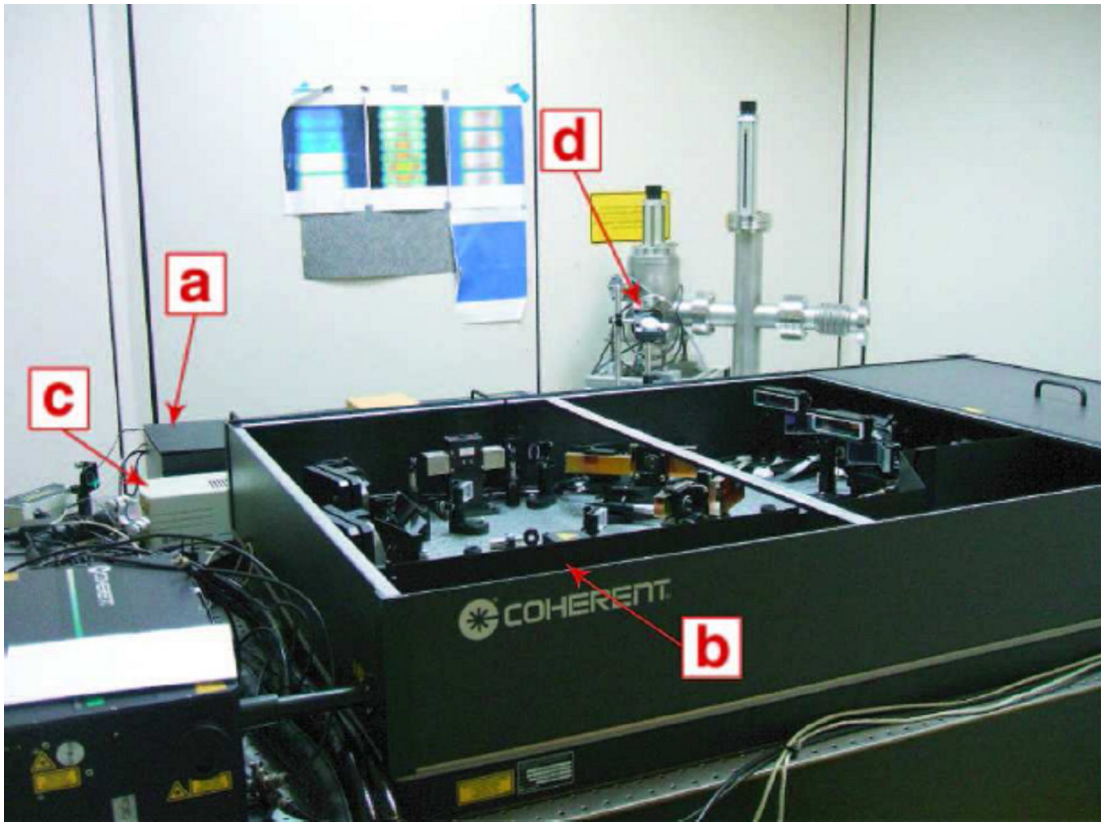

Figure 3.2: The seed laser system. (a) Ti:Sapphire oscillator, (b) Ti:Sapphire amplifier, (c) diode laser and (d) SRFEL back-end viewport.

By second and third harmonic generation in BBO crystals, the wavelength ranges of 390-400 nm and 260-267 nm can also be covered with pulse energies of about 0.8 and 0.3 mJ,

respectively. The peak power is thus high enough for seeding the electron bunch also in the blue and UV. Fig. 3.2 shows the laser system that is located in the FEL back-end station, in a temperature-controlled hutch (see Fig. 3.1c), so as to minimize thermal drifts of the optical alignment. To optimize the energy transfer from the laser to the electron bunch, thus yielding the best micro-bunching with the lowest seed power, the laser pulses must be precisely aligned with respect to the electron bunch both in space and time.

3.4 TIMING

After transverse alignment, the laser must be synchronized to the SR radio-frequency (RF) (= 499.654 MHz) and suitably delayed, so that the seed can temporarily overlap the electron beam inside the modulator. The cavity length of the laser oscillator has been chosen to determine a mode locking frequency as close as possible to RF/6 □ 83.3 MHz. The discrepancy from this value is small enough to be compensated by means of piezoelectric actuator onto which one of the mirrors of the laser cavity is mounted. This action is continuously accomplished by means of a phase locked loop (PLL) logic implemented in the synchronization unit Time-Bandwidth CLX-1100 [19]. If the oscillator is locked to RF/6, the relative phase between the oscillator itself and the single bunch (SB) orbit is constant after every revolution inside the SR. Indeed, the Elettra harmonic number (i.e. the number of RF cycles in an orbit period) is 432, which is divisible by 6. The train of pulses coming from the oscillator enters the regenerative amplifier. The output of the latter (i.e. the seed pulse) is naturally synchronized with the oscillator, but its maximum repetition rate is 1 kHz while the SB revolution occurs at 1.16 MHz. To maintain a constant delay between the seed and the SB orbit every time that the seed pulse is produced, we trigger the Pockels' cells of the amplifier with a period that is an intiger of the orbit period. A scheme of the synchronization setup is shown in Fig. 3.4.

The RF signal is distributed in the experimental hall on coaxial line and is part of the SR "User Timing System" available at Elettra for time resolved experiments. The RF is divided by 6 by means of a low noise eight-channel clock distribution board AD9510 to form the reference signal of the PLL. The PLL is realized by the CLX-1100 unit, which compares the reference signal ($f_1 = RF/6$ □ 83.3 MHz) to the oscillator time structure. The latter is obtained filtering the output signal of a photodiode that collects a spurious reflection of the

radiation stored in the cavity. In this way the phase difference is kept constant and the average phase noise is at sub-ps level, the exact value being determined by the quality of the electrical signals, the environmental condition (e.g. acoustic noise) and the laser stability. To produce the trigger for the amplifier we gate at $f_{amp} = 0.997$ kHz a second output of the AD9510, $f_2 = RF/30 \approx 16.7$ MHz, by means of a delay generator. More precisely, the relationships between the frequencies of the different signals are

$$\begin{aligned} f_{amp} &= f_2/16704 = RF/(30\times 16704) \\ &= RF/(501120) = RF/(432\times 1160) \\ &= f_{SB}/1160 \end{aligned}$$

where f_{SB} is the SB revolution frequency

$$f_{SB} = RF/423 = 1.157 \text{ MHz}.$$

Finally, the amplifier output is delivered every 1160 SB turns. This implies some issues that must be considered in order to separate the CHG from the incoherent synchrotron radiation background that, when integrated over the laser period, can be as intense as the CHG contribution and must be filtered out. For single shot acquisition, the CHG contribution is typically orders of magnitude more intense than spontaneous emission. To trigger the signal shot acquisition we use low jitter (~20 ps) pre-trigger supplied by the amplifier controller unit. In contrast, for integrated measurements we must either subtract the background or develop a gating system for the detection.

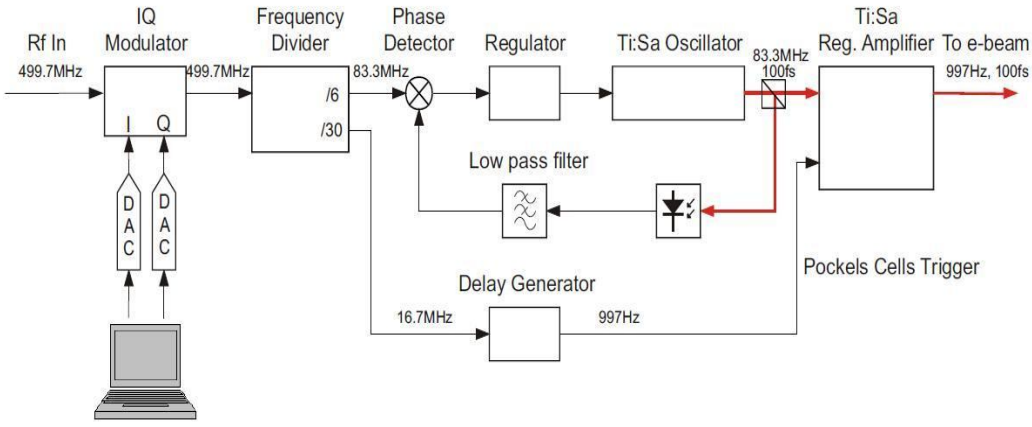

Figure 3.4: Block diagram of synchronization system.

To evaluate and adjust the synchronization between seed and electrons, we proceed as follows. Once aligned in space, the seed beam and the spontaneous emission from the electron beam are collinear. It is therefore possible to collect both signals on a fast photodiode and measure the delay with a broadband sampling oscilloscope. This approach is straightforward and permits a definition of a temporal overlap with an uncertainty better than 20-30 ps, being very close to the electron bunch duration. The most severe limitation is imposed by the great difference in amplitude of the two pulses, the seed being about 10 orders of magnitude above spontaneous emission. Such difference cannot be overcome using optical filters. As a consequence, during this procedure the seed power must be strongly reduced, both to protect the photodiode and to acquire a signal comparable to spontaneous emission. In this condition the seed is not powerful enough to trigger the CHG mechanism. After synchronization, the photodiode is removed and the seed power is increased to the level suitable to initiate the CHG process. A fine optimization of the transverse and longitudinal alignment is made maximizing the intensity of the produced harmonics. To continuously monitor the stability of the synchronization during harmonic generation once the generation process is optimized, we can calibrate an indirect indicator for the longitudinal alignment. The SR User Timing System includes the distribution of the signal from the “pick-up electrode”. The latter is obtained by amplification of the signal from an inductive electrode placed in the SR vacuum chamber. For SB filling, this procedure produces a sharp spike (~200 ps of rise-time) that indicates the relative position of the bunch inside the ring. The delay that we measure between the seed pre-trigger and this signal when the CHG is optimized depends only on the laser optical path and on the coaxial line length. Such a delay is a reproducible quantity, thus avoiding repeating the delicate and time-consuming synchronization procedure based on the use of the photodiode.

To adjust the phase shift between the seed and the electron beam and to obtain a suitable longitudinal alignment, we use a digital IQ vector modulator based board. This low noise device introduces an arbitrary phase shift on the RF reference signal. If the phase shift is small enough, the corresponding delay is propagated throughout the electronics (AD9510 divider and PLL) to the oscillator pulses without losing the locking condition. Empirically, we observed that it is possible to shift the pulse train with respect to the electrons with a speed of the order of 100 ns/s maintaining the locking condition.

The amplitude and phase noise of the RF signal have been measured with an Agilent Source Signal Analyzer. The integrated absolute jitter is about 1.5 ps RMS in the 10 Hz to 10 MHz offset frequency range. For the typical electron bunch length, this value is small enough to ensure a correct synchronization. The final jitter on the pulse train of the oscillator is 2.6 ps RMS mostly due to the RF jitter and oscillator instability. In fact, we have estimated the contribution to the total jitter of the IQ modulator and the AD9510 divider to be 50 and 250 fs, respectively. If used with a state-of-the-art low jitter reference signal (few tenth of fs) and femtosecond fiber oscillator, this setup can be applied when timing stability requirements are more severe, as is the case of the seeding of next-generation, linac-based, seeded CHG sources.

3.5 DIAGNOSTICS

The light emerging from the front-end exit is transmitted inside the front-end hutch passing through a CaF_2 view-port that separates the SR UHV area from the atmosphere. Here the light is detected and characterized by means of a 750 mm, Czerny-turner design spectrometer. This instrument mounts two UV-blazed gratings, one for medium dispersion (i.e. 6001/mm) and the other for high dispersion (36001/mm). After dispersion, the light can be focused either onto a liquid nitrogen cooled charge-coupled device (CCD) detector or, by means of a side mirror, on the exit after which a photo-multiplier tube (PMT) is mounted. The layout of the diagnostics used to characterize the harmonic radiation is shown in Fig. 3.5.

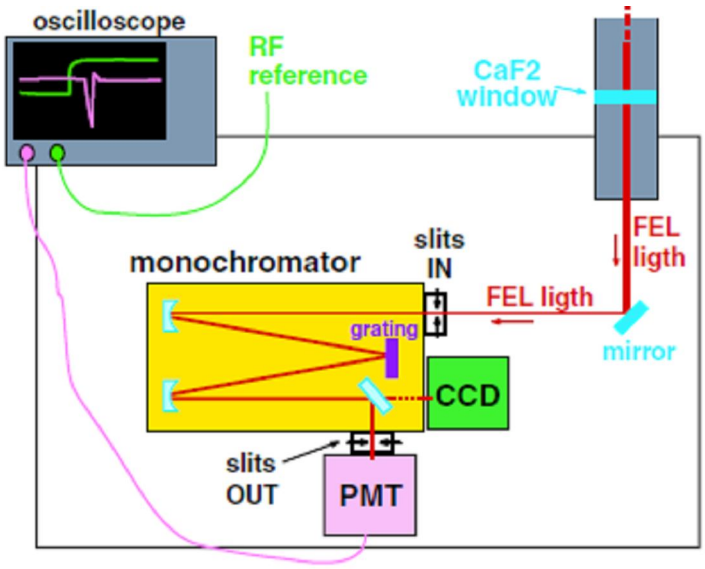

Figure 3.5: Layout of the detection area.

In a single acquisition the CCD can record a whole spectrum whose width depends on the grating in use. It is suitable for very weak intensity but the minimum integration time is about 50 ms, which is much longer than the laser period. For this reason, in order to extract the contribution of the harmonic emission only we need to acquire and subtract the background of spontaneous emission.

The PMT is a single channel detector with good detection efficiency and fast response (rise time ~ 1 ns). It is used for single shot measurements in a given bandwidth that depends on the grating dispersion and on the width of the exit slits.

The light can also be transported outside the hutch and focused into an experimental end-station (see Fig. 3.1b). In the optical path we can insert different sets of interferential mirrors that allow separating and recombining harmonics and seed. This permits to optically delay one signal with respect to the other to perform pump and probe experiments. The optical path, from the CaF_2 window to the end-station and trough the spectrometer can be purged with N_2 flow in order to reduce the atmosphere's absorption in the UV range.

The SRFEL beamline shares with the Nanospectroscopy beamline the optical klystron in the Elettra straight section 1. The transport of the harmonic pulses produced in the FEL branch is accomplished by means of a switching mirror.

STREAK CAMERA

A streak camera is an instrument to measure very short optical pulses in a wide spectral range. A pico-second resolution double-sweep streak camera (DSSC) [20] is used to measure and characterize the electron beam and FEL properties. By measuring the visible part of the optical pulse generated by electrons passing through a bending magnet (synchrotron radiation) it is possible to infer the bunch length and also the electron beam stability. Fig. 3.6 shows a picture of the double sweep streak camera used for our measurements.

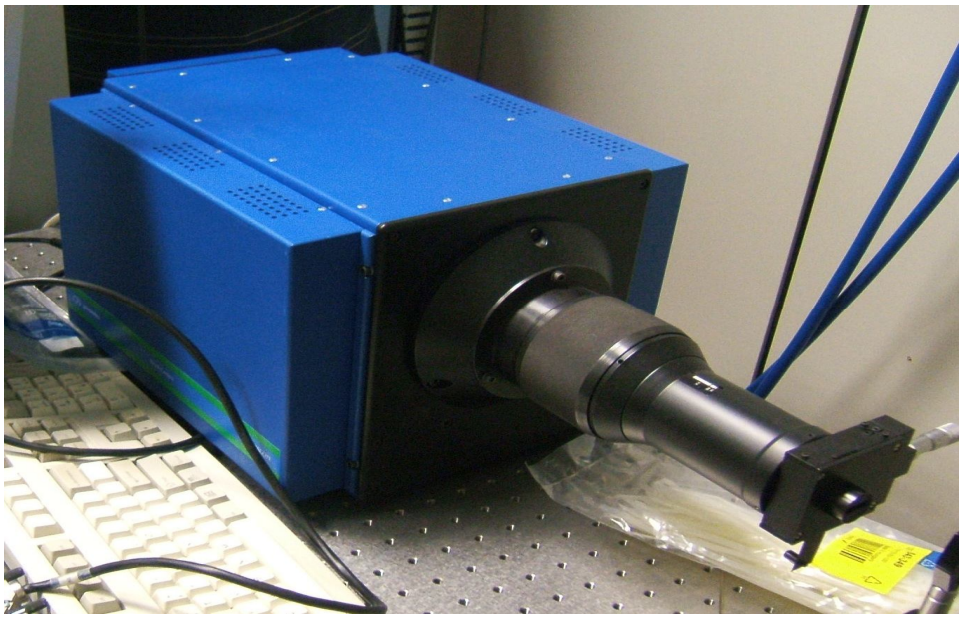

Figure 3.6: Picture of a double sweep streak camera.

The DSSC working principle is shown in Fig. 3.7 and it relies on a time-to-space conversion of the fast optical pulses. The focused incoming photons are converted into electrons by a photocathode. The emitted electrons are accelerated and deflected by a high voltage applied to the deflection electrodes. A charge-coupled device (CCD) camera acquires the streaked-out final image on a phosphor screen generated by these electrons, placed at the instrument end. The streak camera detects the light emitted from bending magnets as a function of time, with resolution of about 3 ps. The fast time acquisition (0-300 ps range) is displayed on the horizontal axis. Consecutive short time acquisitions are displayed along the vertical axis (the range is 0-42 ms).

By combining the synchrotron radiation and the FEL pulses, the DSSC acquisition is able to provide information on the coupled electron-laser dynamics.

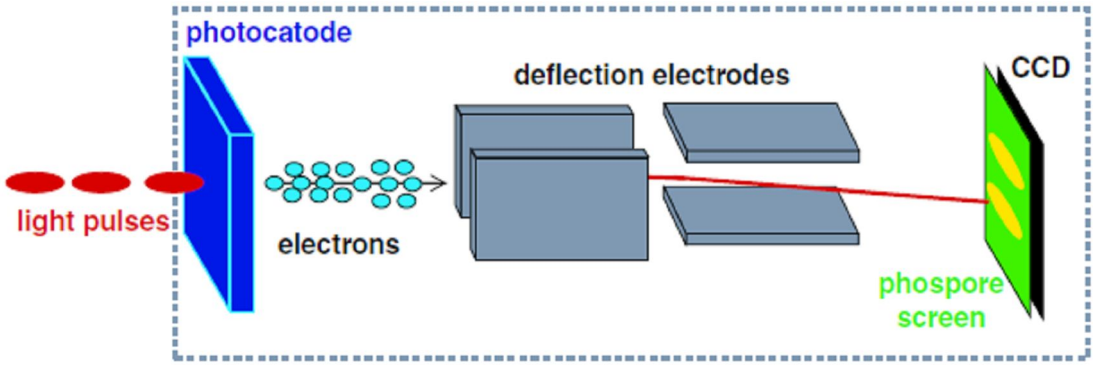

Figure 3.7: Working principle of a double sweep streak camera. The light pulses are converted by the photocathode into electrons that pass through two orthogonal pairs of deflection electrodes. The deviated electrons are then collected by a phosphor screen and a linear detector, (such as a CCD array) is used to measure the pattern on the screen and thus the temporal profile of the light pulse.

4 GENERATION OF COHERENT HARMONICS

In this Section we present the experimental performance obtained in seeded configuration with the Elettra optical klystron. Taking advantage of the SR FEL beamline and, in particular, of the already implemented experimental setup for CHG (see Chapter 3), we generated FEL radiation at 195 nm and 87 nm, using different experimental settings. As was already mentioned, the generation of coherent light at 87 nm is a major achievement: in fact, at present this is the shortest wavelength ever reached using an FEL based on a seeded scheme. In the following, we present the observed experimental performance of the harmonic radiation.

4.1 CHARACTERIZATION OF FEL PULSES AT 195 nm

The experiments for the production and characterization of FEL pulses at 195 nm have been performed setting Elettra at an electron energy of 750 MeV.

The reason for using a beam energy lower than nominal (900 MeV) is that we tried to make the FEL operational for future experiments at the fundamental wavelength of the seed laser (780 nm). In fact, recalling the resonant condition, Eq (2.28), one can see that the undulator strength is limited by the minimum gap at which the undulators can be closed. The latter is determined by the aperture of the vacuum chamber where the electrons circulate. In the case of the Elettra SRFEL section, such an aperture is 19 mm. This does not allow to tune the modulator to 780 nm when Elettra operates at 900 MeV. Hence, to reach the resonance condition at 780 nm we needed to reduce the energy of the electron beam down to 750 MeV. As we pointed out in Section 3.2, when Elettra is operated at energies lower than 900 MeV, the electron beam instabilities may be particularly harmful.

The repetition rate of the seed laser and, as a consequence, of the coherent pulse is 1 kHz. For the experiment we performed, the wavelength of the seed laser is 390 nm, with a power of 4.5 GW (this is the second harmonic of the fundamental wavelength of the seed laser). We tuned the modulator to the wavelength of the seed laser (390 nm) and the radiator to the wavelength of its second harmonic (195 nm).

4.1.1 MEASURMENTS OF SPECTRAL PROFILE

The spectral profile of the FEL signal at 195 nm has been measured using the setup described in Section 3.5.

The result is shown in Fig. 4.1. The electron-beam current was 1.1 mA. As it will be shown in the next Section, when compared to spontaneous (incoherent) synchrotron radiation, the seeded CHG technique allows to gain a factor $10^2 - 10^3$ in terms of photons per pulse. Unfortunately, as already stated, the repetition rate of the harmonic pulses is limited to 1 kHz by the seed laser, i.e. three orders of magnitude less than the repetition rate of spontaneous emission. Moreover, the acquisition time of the CCD coupled with the spectrometer is in the ms range. This is the reason why in Fig. 4.1 the spontaneous emission is comparable to the CHG signal.

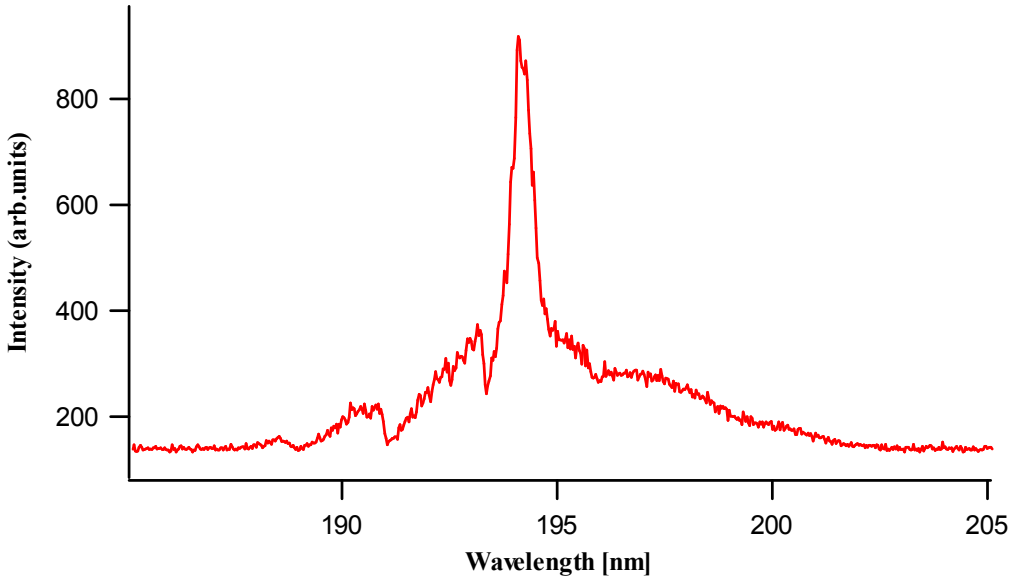

Figure 4.1: The averaged spectrum of coherent harmonic radiation at 195 nm. One CHG pulse corresponds to about one thousand round trips of the electron beam and, hence, to one thousand pulses of (spontaneous) synchrotron radiation.

To get a better notion of the pulse, it is useful to remove the background noise that is produced by spontaneous emission of the electron bunch. This provides the net CHG contribution. The signal after the subtraction of the unseeded contribution, and the unseeded contribution itself, are shown in Fig. 4.2. Background noise may be a trouble when the light is

exploited for user experiments. The problem can be solved by "gating" the emitted radiation, i.e. selecting only the seeded light.

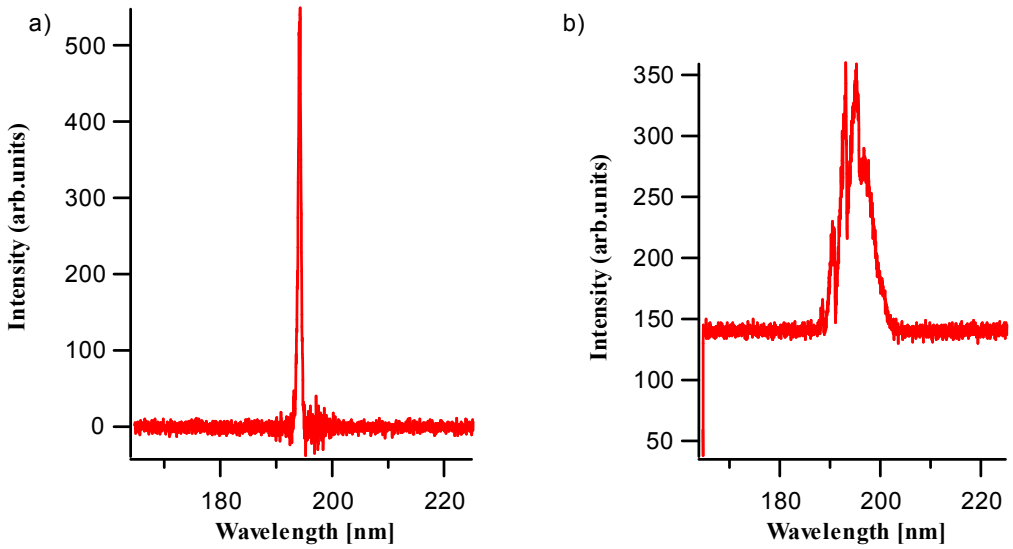

Figure 4.2: (a) The harmonic emission spectrum obtained after background subtraction (spontaneous emission) and (b) the background itself.

The estimation of the spectral width of the CHG signal gives a bandwidth $\Delta\lambda$ of about 0.39 nm FWHM. If we assume for the harmonic the same pulse duration of the seed pulse (100 fs FWHM), this value is 1.4 times above Fourier limit[4], the latter being determined according to the following relation

$$c\Delta t \frac{\Delta\lambda}{\lambda^2} \geq 0.441 \qquad (4.1)$$

(where c is the speed of light), which is quite a good result. Indeed, this means that the signal is as "monochromatic" as the temporal duration allows.

4.1.2 NUMBER OF PHOTONS PER PULSE

We estimated the number of photons in the CHG pulse by comparing it with the spontaneous emission. This was done with the SPECTRA 8.0 [21] program giving the flux (i.e. the number of photons per second contained in 0.1 % of the bandwidth) of spontaneous emission. The

[4] In ultrafast optics, the Fourier limit (or transform limit) is usually understood as the lower limit for the pulse duration for a given optical pulse spectrum.

relevant parameters used in this program were the same as in the experimental setup (see Table 3.1 and Table 3.2).

The result is $\text{Flux} = 1.34 \times 10^{12}$ (ph./sec./0.1%bw). To get the flux over the entire bandwidth we multiply this result by a factor 1000, $\text{Flux} = 1.34 \times 10^{15}$ (ph./sec./bw).

The relative bandwidth of the undulator is given by the formula

$$\frac{\Delta\lambda}{\lambda} = \frac{1}{N}, \tag{4.2}$$

where N is the number of undulator periods. Thus, $\frac{\Delta\lambda}{\lambda} = \frac{1}{20} = 0.05$. The frequency of the electron bunch is $f_{synchr} = 1\text{MHz}$. The number of photons per pulse of the spontaneous emission over the whole bandwidth is then

$$\frac{Flux(ph./\sec./bw)}{f_{synchr.}} \frac{\Delta\lambda}{\lambda} = 6.7 \times 10^{7}. \tag{4.3}$$

The integral over the pulse in Fig. 4.2a gives the area of the CHG pulse, $A_{CHG} = 11609.7$ (arb.units). From the integral in Fig. 4.2b, divided by the ratio between synchrotron radiation and CHG repetition rates (1000), we get the area of the spontaneous emission signal, $A_{SE} = 324.4$ (arb.units). Finally, the number of photons in one CHG pulse is given by:

$$\left(\frac{A_{CHG}}{A_{SE}}\right) \frac{Flux(ph./\sec./bw)}{f_{synchr.}} \frac{\Delta\lambda}{\lambda} = 2.4 \times 10^{9}. \tag{4.4}$$

4.1.3 TIME RESOLVED MEASURMENTS

The coherent harmonic radiation is monochromatized and then acquired on a digital oscilloscope by means of a PMT (see Section 3.5), fast enough to resolve the pulse dynamics of emission from a single electron bunch, but does not allow to resolve the real photon pulse shape.

In Fig. 4.3 the acquired temporal signal at 195 nm is shown. The high peak represents the coherent signal generated by the FEL in seeded configuration, while the small peaks at both sides reproduce the spontaneous emissions of the electron bunch passing through the undulator. As before, the electron beam energy is 0.75 GeV. The current of the bunch is in this case 1.4 mA.

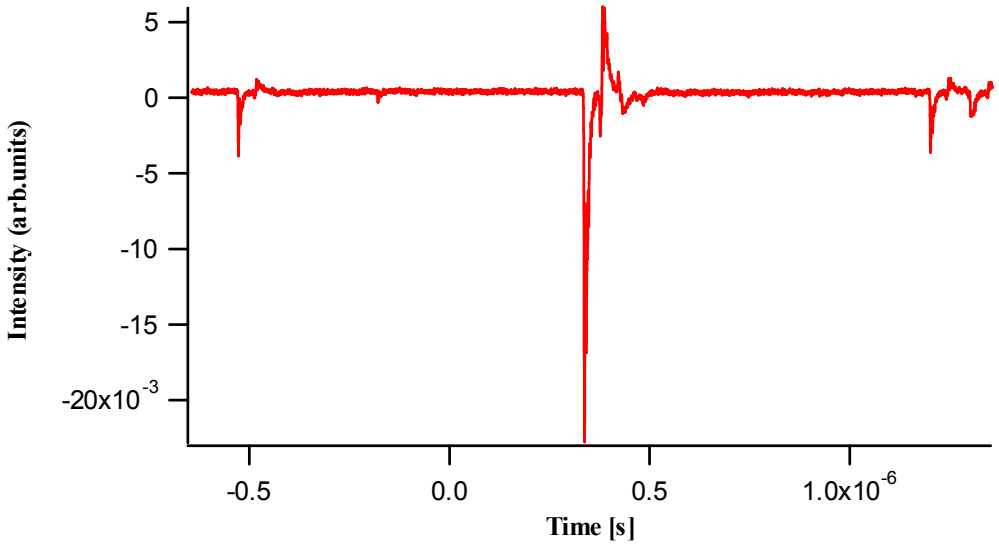

Figure 4.3: Signal at 195 nm as a function of the acquisition time.

4.2 DISPERSIVE SECTION SCAN

In Fig. 4.4 we report the optimization of the dispersive section in order to maximize the harmonic signal. By changing the current that powers the dispersive section, while keeping the seed power fixed, we observed a change in the intensity of the harmonic signal over time. The scan begins at 3 A (almost zero intensity) and ends at 200 A, where the intensity drops down to zero again. We found the optimum value around 120 A (represented by the peak in the graph). Above 120 A, the trend of intensity shows that the beam goes in overbunching.

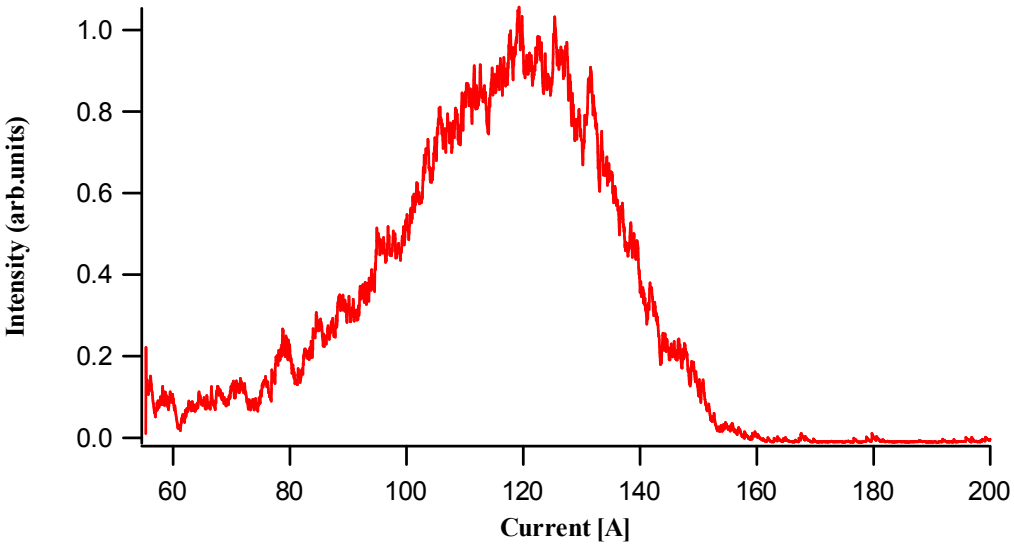

Figure 4.4: Harmonic intensity at 195 nm vs. dispersive section strength.

4.3 ELECTRON BEAM CHARACTERIZATION

We also characterized the dynamics of the electron beam, both in the presence and in the absence of the FEL. This was achieved with the use of the streak camera (see Section 3.5).

The streak camera images in Fig. 4.5 represent the electron bunch in the absence of interaction with the seed laser (at current 0.35 mA). Performing an analysis of the of the streak camera image, shown in Fig. 4.5a, it is possible to follow the evolution of the bunch length and the position of the beam center of mass over the "slow" acquisition time. This helps to determine the beam stability. Fig. 4.5b displays the bunch-length profile, obtained by performing a horizontal cut on Fig. 4.5a. Performing a Gaussian fit we get a bunch-length of 23.3 ps. We see that the bunch profile is almost Gaussian. This is a direct proof of the fact that the electron beam is not perturbed by instabilities due to wake fields i.e. electromagnetic fields produced by the electrons interaction with the metallic beam pipe. Fig. 4.5c shows the evolution of the electron-beam (rms) duration over the "slow" acquisition time: the obtained curve demonstrates the relatively good stability of the bunch duration, whose average value is 23.1 ps.

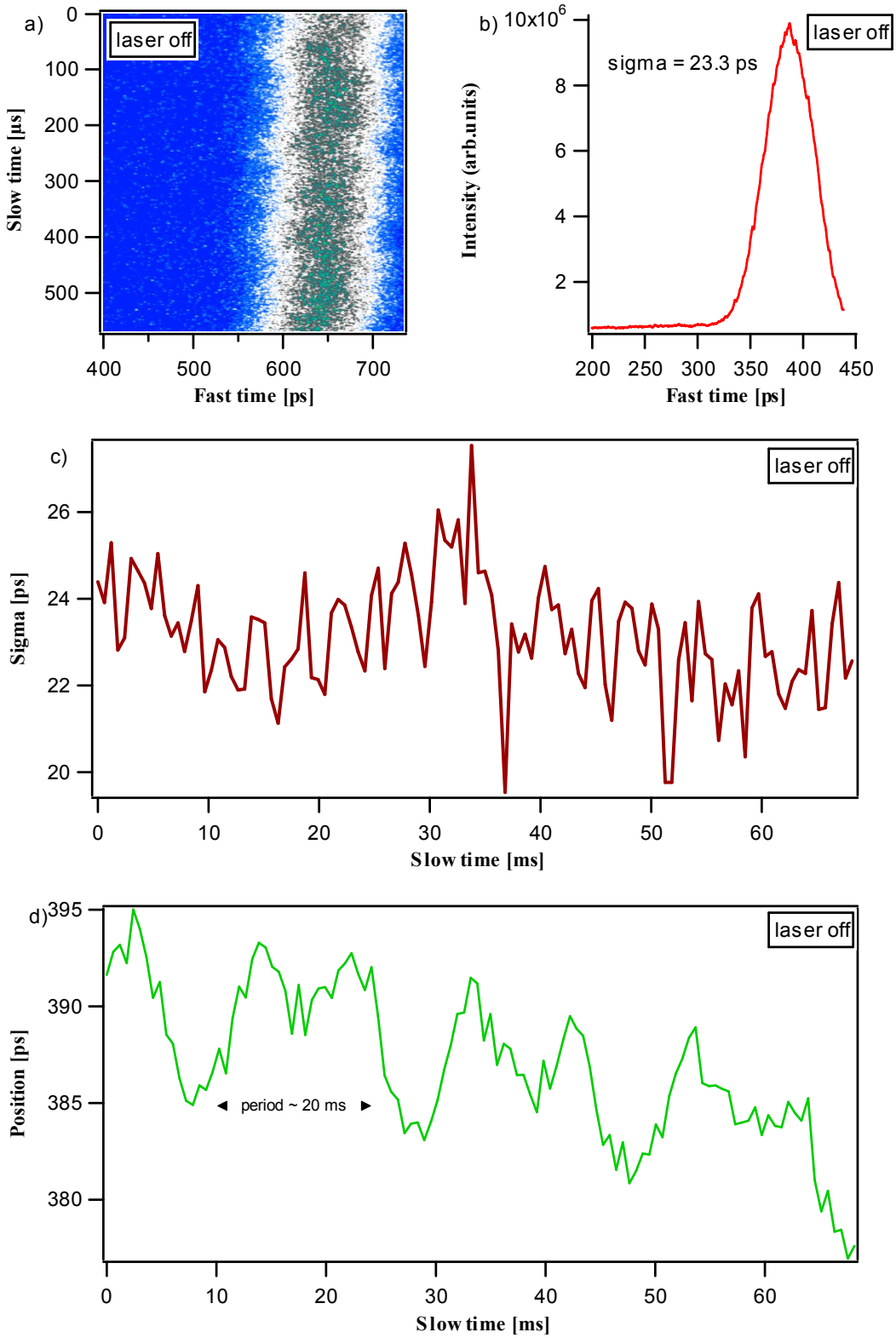

Figure 4.5: (a) Streak camera image at 0.75 GeV in the absence of seed-electron interaction. (b) Measurements of the bunch-length and (c) its evolution, obtained performing a horizontal cut on the streak image. (d) Evolution of the electron-beam centroid obtained by performing a vertical cut on streak image. The current is 0.35 mA.

A vertical cut of Fig. 4.5a provides the evolution of the electron-beam centroid. The measurement, shown in Fig. 4.5d, demonstrates that the electron beam is not perfectly stable: the centroid displays a periodic instability with a period of about 20 ms (50 Hz). The source of this perturbation is not fully understood and is probably related to some instabilities of the power supplies of one or more Elettra magnets.

We performed bunch-length measurements during CHG (laser on) at current 0.45 mA. A comparison of seeded/unseeded bunch length at this current is shown in Fig. 4.6. One can observe a lengthening of the bunch in a presence of the laser.

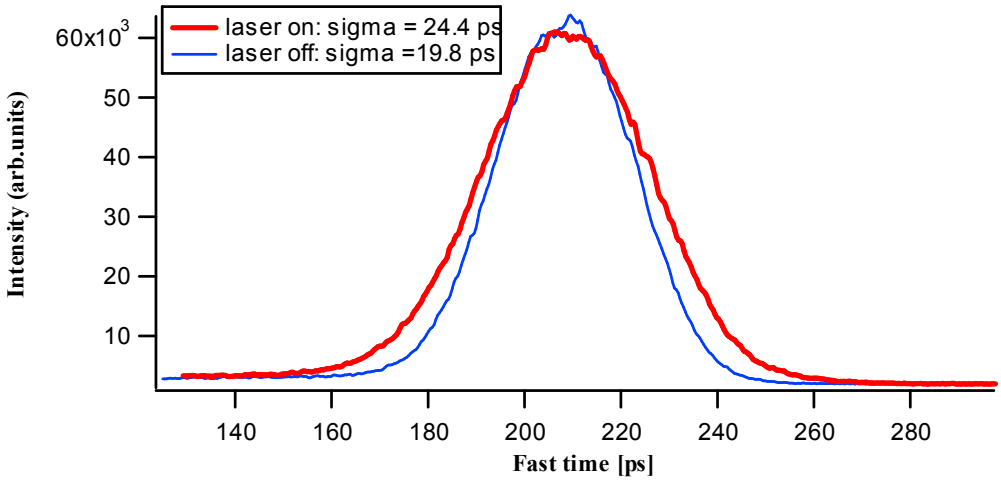

Figure 4.6: Comparison between seeded and unseeded bunch length. The current is 0.45 mA.

4.4 COHERENT EMISSION AT 87 nm (14.2 eV)

In this section we report about the most important result we obtained during my experimental activity at Elettra: the generation of a coherent signal at 87 nm (third harmonic of a seeding signal at 261 nm, having a peak power of 1.5 GW). The relevance of this result lies in the fact that this is presently the shortest wavelength ever reached on a seeded free-electron laser. For this experiment, Elettra was operated at 0.9 GeV.

The evidence of CHG at 87 nm has been obtained during the late shift of May 11th, 2009. In order to measure the spectral distribution of the CHG radiation, the SPELEEM (Spectroscopic PhotoEmission and Low Energy Electron Micoscope) installed at the Elettra Nanospectroscopy beamline (see Fig. 3.1) was used to observe the photo-electron yield from an Au thin-film, as a function of the photon energy.

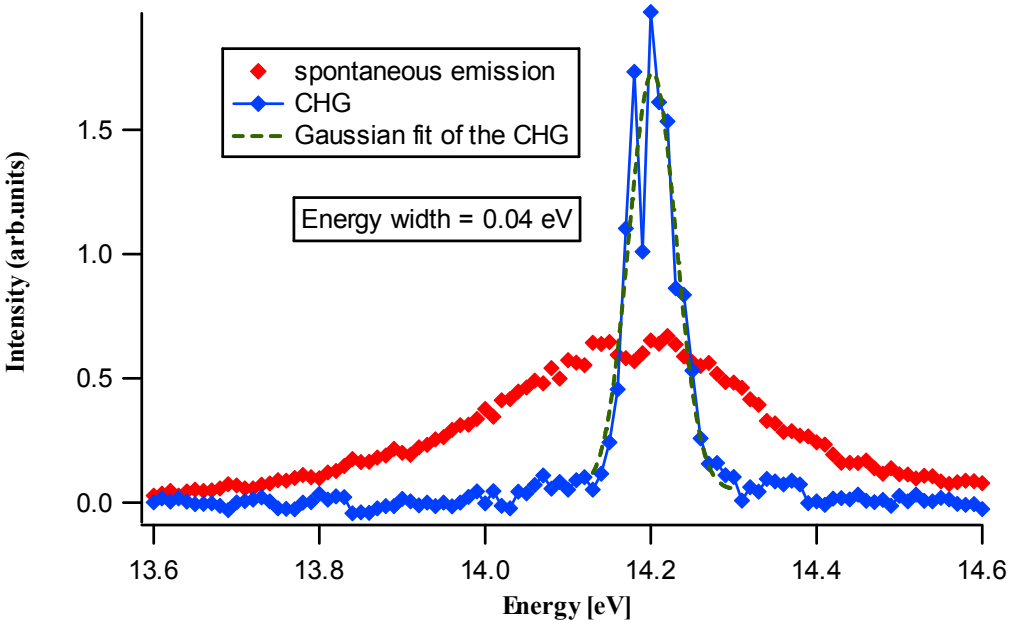

Figure 4.7: The third harmonic of the seed laser (87 nm), together with the spontaneous emission and a Gaussian fit of the CHG. The detector was gated in order to acquire only the emission from seeded bunch.

The resulting spectrum of this experiment is presented in Fig. 4.7. The Gaussian fit of a CHG gives an energy width of about 0.04 eV. This quite large value, about 2.8 times that Fourier limit, is due to the low resolution (at these wavelengths) of the spectrometer installed at the Nanospectroscopy beamline.

4.4.1 THE NUMBER OF PHOTONS PER CHG PULSE

The estimation of the number of photons per pulse has been done comparing the coherent signal to the spontaneous emission. The synchrotron radiation generated by one undulator has been estimated using the SPECTRA 8.0 software. Using the parameters reported in Table 3.1 and 3.2, this program gives the flux of 1.34×10^{12}(ph./sec./0.1%bw). The relative bandwidth of one undulator and the frequency of the electron bunch are the same as in the previous case (see Section 4.1.2: $\frac{\Delta\lambda}{\lambda}=0.05; f_{synchr}=1\text{MHz}$).

The integral of the area of the spontaneous emission form Fig. 4.8 gives us the value $A_{SE}=28.0$ (arb.units) and of the CHG area as $A_{CHG}=14.1$ (arb.units). Here we do not have to

divide the area of the synchrotron radiation by the ratio between synchrotron radiation and CHG repetition rates, as we did for the case at 195 nm, since, the measurement was gated and only the radiation from the seeded bunch was acquired. The number of photons in one CHG pulse is given by Eq. (4.4) and is 3.3×10^{7}.

As we can see, the number of photons per CHG pulse and that of the spontaneous emission is very similar. However, the CHG signal is concentrated in a much shorter time (100 fs compared to 30 ps of the spontaneous emission). This gives a much higher peak power for the CHG. We also see in Fig. 4.7 that the CHG signal is concentrated in a significantly smaller bandwidth; meaning that if the signal is monochromatized, i.e. the tails of spontaneous emission are filtered out, another significant factor can be gained.

5 LAYOUT AND GENESIS SIMULATIONS

To get a complete characterization of the coherent harmonic radiation, we carried out detailed simulations using the tri-dimensional FEL code GENESIS [22]. The aim was to reproduce the experimental results, understand the role of the main parameters and also possibly find improvements to the FEL performance.

In GENESIS, the electron beam is represented by macroparticles propagating in their 6D phase space (x, y, z, p_x, p_y, p_z). Simulations can be run either in time-dependent or time-independent mode. Time-independent simulations are based on the assumption of an infinitely long electron bunch and radiation field with no longitudinal variation of any parameter. The time-dependent simulations take into account the finite duration of the electron beam, the possible variations in its longitudinal (with current and energy) and transverse shapes, as well as the longitudinal shape and the spectrum of the FEL pulse.
The "thermalization" of the electron-beam properties due to the multi-turn dynamics in the storage ring results in a very good reproducibility of the seeding process (see Section 3). As a consequence, we do not expect a significant difference between predictions obtained in time-independent or time-dependent mode.

We start with the simulations of CHG at 87 nm and then we present the results at 195 nm. The main parameters used to simulate the Elettra FEL are shown in Table 5.1. A description of GENESIS input files is reported in Appendix A.

Table 5.1: Elettra parameters used in GENESIS calculations.

Energy (GeV)	0.75-0.91
Current range (mA)	10 A-76 A
Natural" (i.e. low-current) RMS Emittance at 0.9 GeV	1.74 nm rad
"Natural" (i.e. low-current) RMS energy-spread	0.12% at 0.9 GeV 0.23% at 0.75 GeV
"Natural" (i.e. low-current) RMS bunch-length	5.4 ps at 0.9 GeV 4.1 ps at 0.75 GeV

5.1 SIMULATIONS OF CHG at 87 nm

Here we report the simulations aimed at reproducing the results of the CHG experiment at 87 nm.

5.1.1 PRELIMINARY (TIME-INDEPENDENT) CALCULATIONS

The purpose of these preliminary simulations is to find the values of the seed power, dispersive section strength, modulator and radiator wavelengths at which the optimal output radiation power are obtained. For this reason, we run a large number of simulations with slightly different (randomly varying) values of the above mentioned parameters, and observed the obtained output power. All parameters are varied at the same time.

The central power of the seed is 1 GW, with random values generated in the range from 0 to 2 GW. In Fig. 5.1 the power emitted at the end of the radiator at the third harmonic (87 nm) is plotted versus the power of the seed laser.

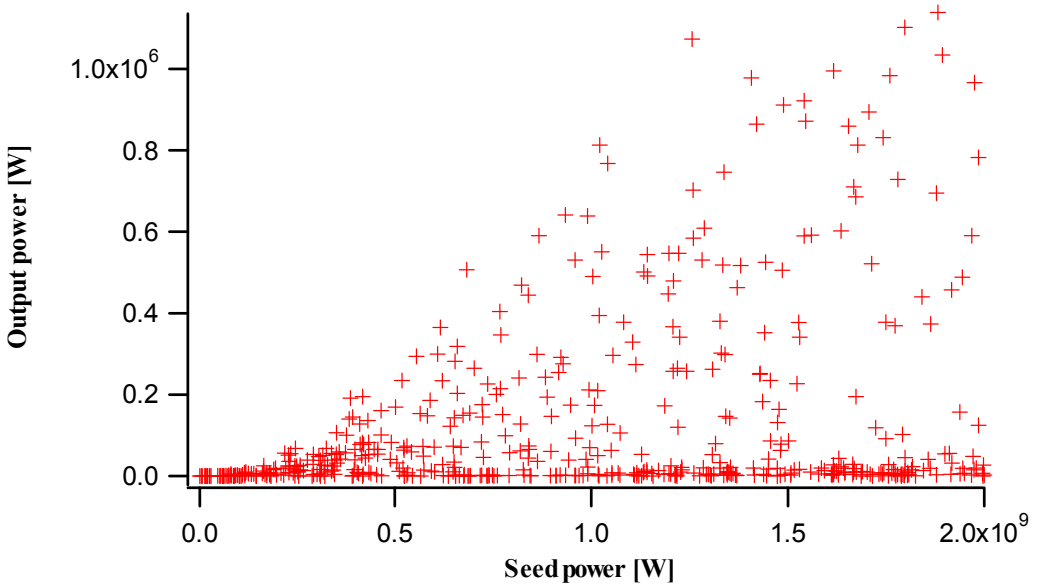

Figure 5.1: Output power at 87 nm as a function of the seed power at 0.9 GeV.

From this figure we can se see that the power of the radiation is growing with the seed power. This means that the seed power is not strong enough to induce the overbunching of the electron beam.

In Fig. 5.2 we show the results on the dependence of the output power on the dispersive section strength. We see a peak in the graph, after which the beam goes in overbunching.

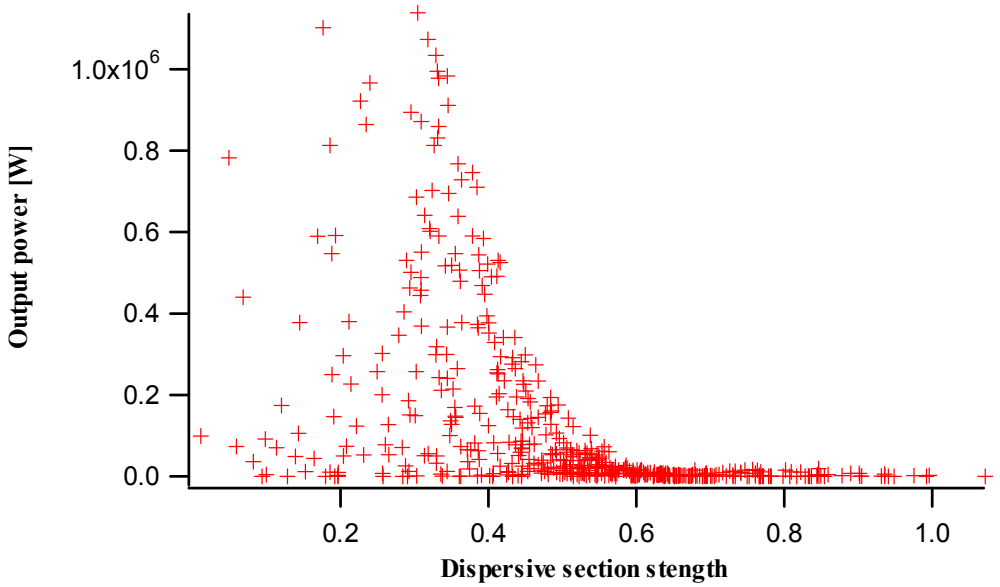

Figure 5.2: Third harmonic power as a function of the dispersive section strength (in "GENESIS" units).

Fig. 5.3 shows the output power with respect to the modulator wavelength.

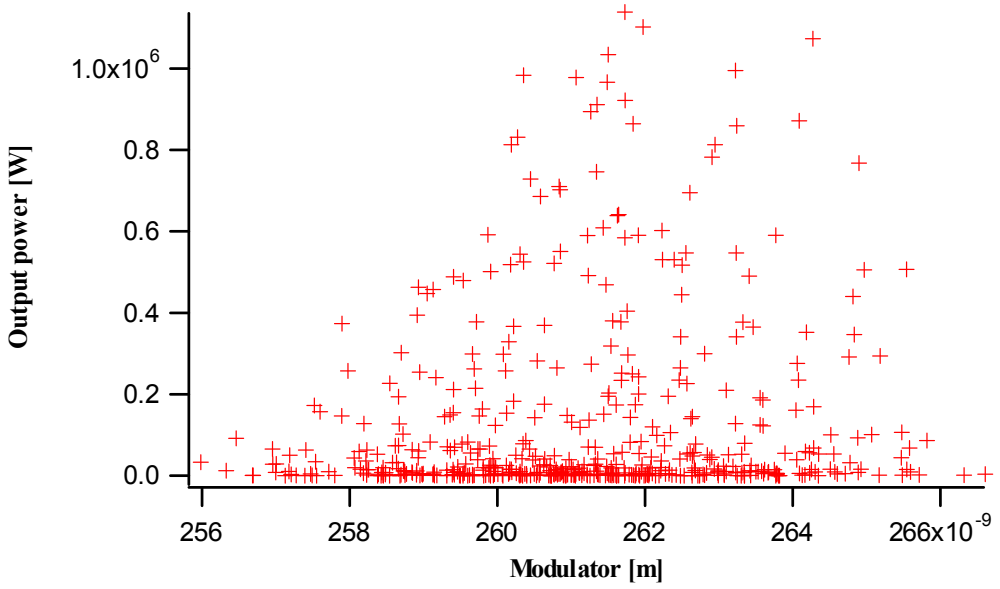

Figure 5.3: The output power as a function of the tuned wavelength of the modulator.

The performance of the output power at different radiator wavelengths is shown in Fig. 5.4.

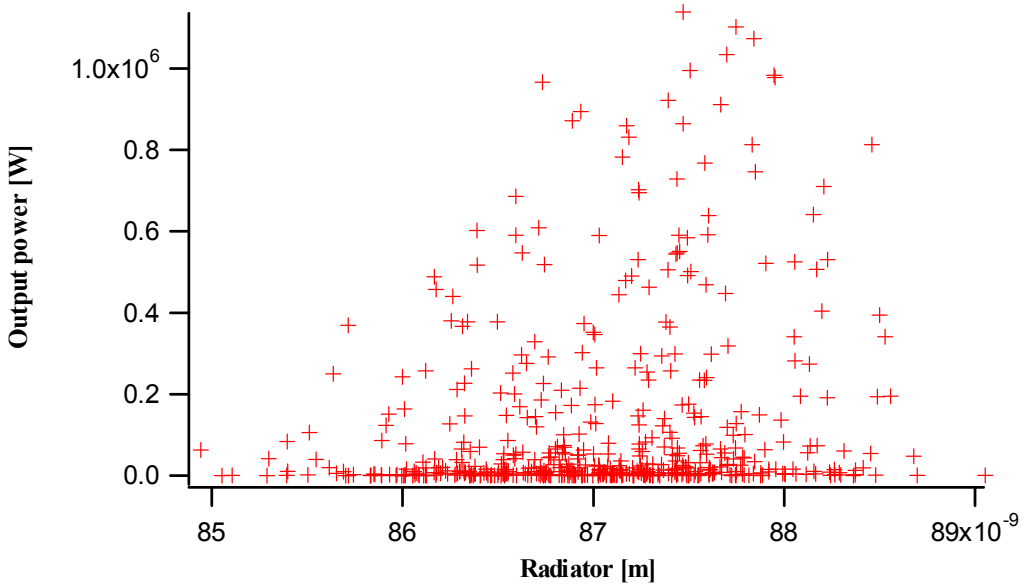

Figure 5.4: The output power as a function of the tuned wavelength of the radiator.

Predictably, the highest output power for the modulator is close to 261 nm and for the radiator is close to 87.

5.1.2 EXPECTED PERFORMANCE: TIME-INDEPENDET MODE

We performed simulations in time-independent mode using the optimum values obtained from the preliminary calculations. During experiments, we operated with a seed laser power of 1.5 GW. Taking that into account, we selected the optimum value of the seed power and the corresponding values of the dispersive section strength, modulator and radiator wavelengths. Such values are reported in Table 5.2. Appendix B gives the input files for this simulation.

Table 5.2: Main parameters used to find the optimum output power. For the reported simulations, the electron-beam energy is fixed at 0.9 GeV and the peak current is 76 A.

Seed Power (GW)	1.48
Modulator Wavelength (nm)	261.35
Radiator Wavelength (nm)	87.67
Dispersive Section Strength (mm)	0.34

Fig. 5.5a shows the evolution of the bunching (at the seed wavelength) along the modulator and Fig.5.5b shows the evolution of the bunching (at the harmonic wavelength) along the

radiator. The trend of the latter curve shows that the saturation is reached inside of the first part of the radiator.

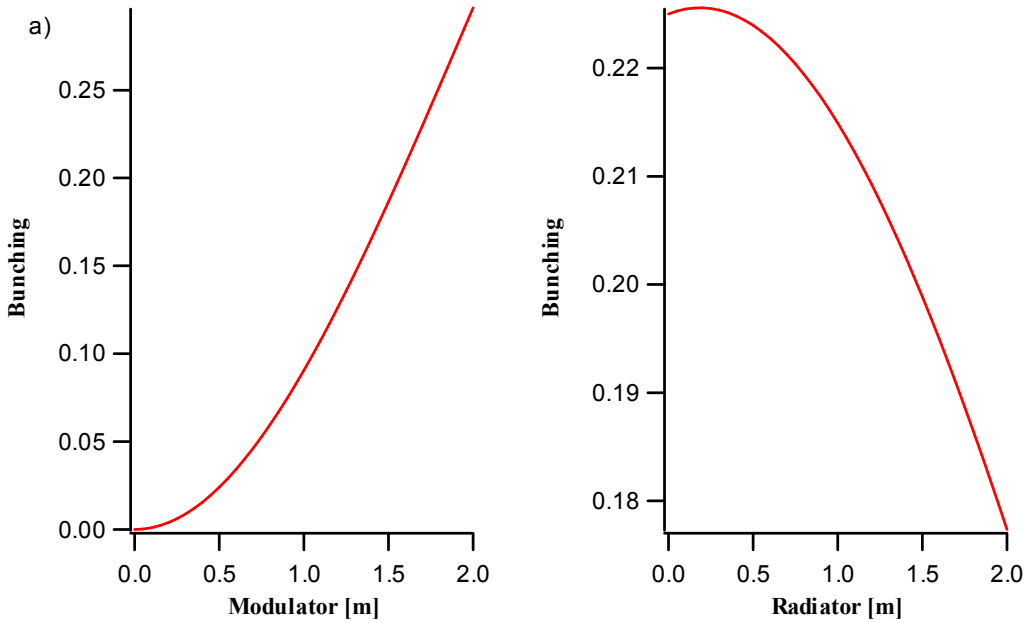

Figure 5.5: (a) Evolution of the bunching along the modulator and (b) along the radiator.

The third harmonic output power along the radiator is shown in Fig. 5.6. In spite of the fact that the bunching saturates (see fig. 5.5), the radiator length is not sufficient to reach the power saturation.

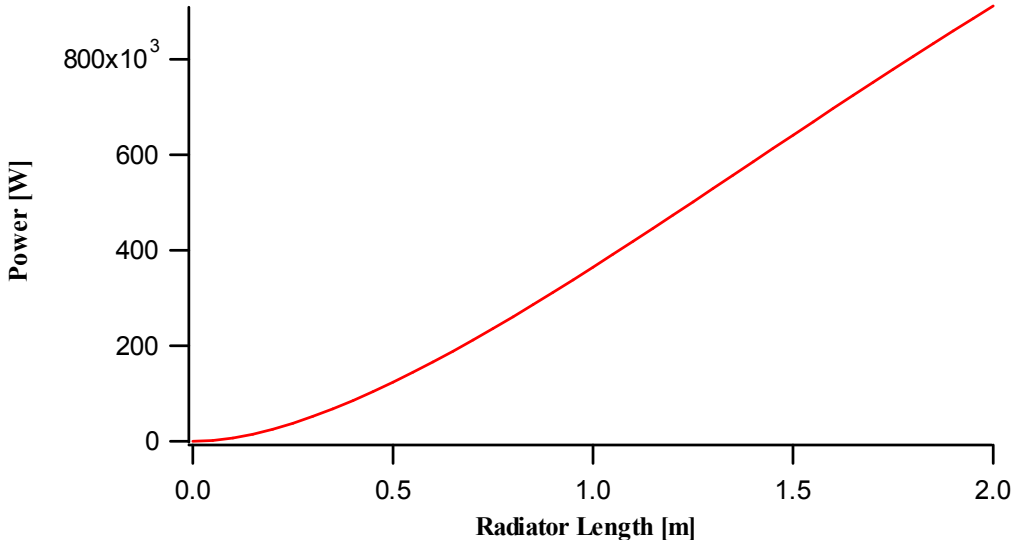

Figure 5.6: Output power along the radiator at 87 nm.

5.1.3 EXPECTED PERFORMANCE: TIME-DEPENDENT MODE

The "best case" (corresponding to the parameters reported in Table 5.2) has been simulated using GENESIS in time-dependent mode. The electron beam energy is 0.9 GeV, the peak current is 10 A and the bunch duration is 30 ps.

For the seed laser we assumed a Gaussian profile with peak power of 1.48 GW, see Fig. 5.7.

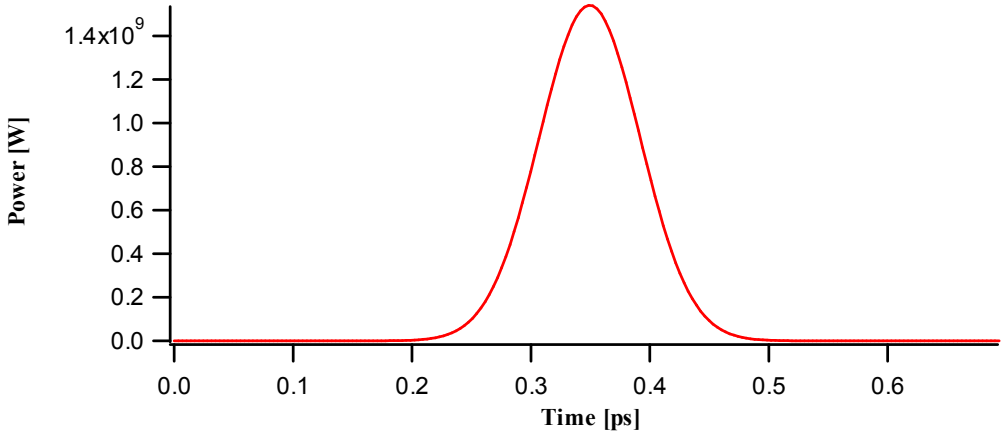

Figure 5.7: The temporal profile of the seed laser.

Because we are interested only in what happens to the seeded part of the bunch, we simulated just a small part of it (only 600 fs).

The bunching evolution inside the modulator is shown in Fig. 5.8. Fig. 5.8a shows the bunching at the beginning of the modulator (before interaction with the seed). The bunching at the end of the modulator (after interaction with the seed) is shown in Fig. 5.8b. From this we can see the effect of the beam interaction with the seed laser: from a random distribution of the electrons at the entrance of the modulator we get an "ordered" state.

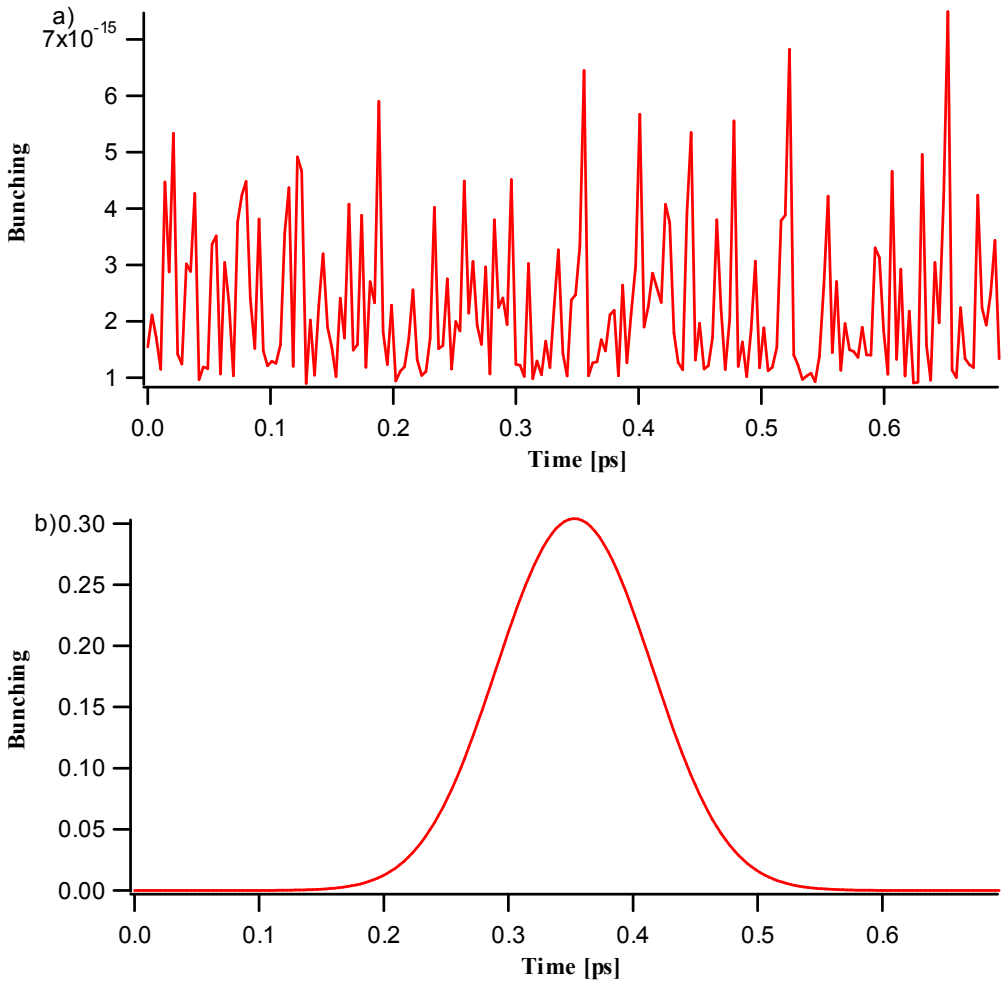

Figure 5.8: (a) Bunching at the beginning and (b) at the end of the modulator.

In Fig. 5.9a we report the spectrum of the third harmonic signal at the radiator exit. The temporal profile of the harmonic signal is shown in Fig. 5.9b. We see that the output power is about 15 kW. Analyzing the spectral profile we calculated the number of photons in one harmonic pulse at 87 nm. The number is 5.2×10^{8}. This will later be used in a comparison with the experimental result.

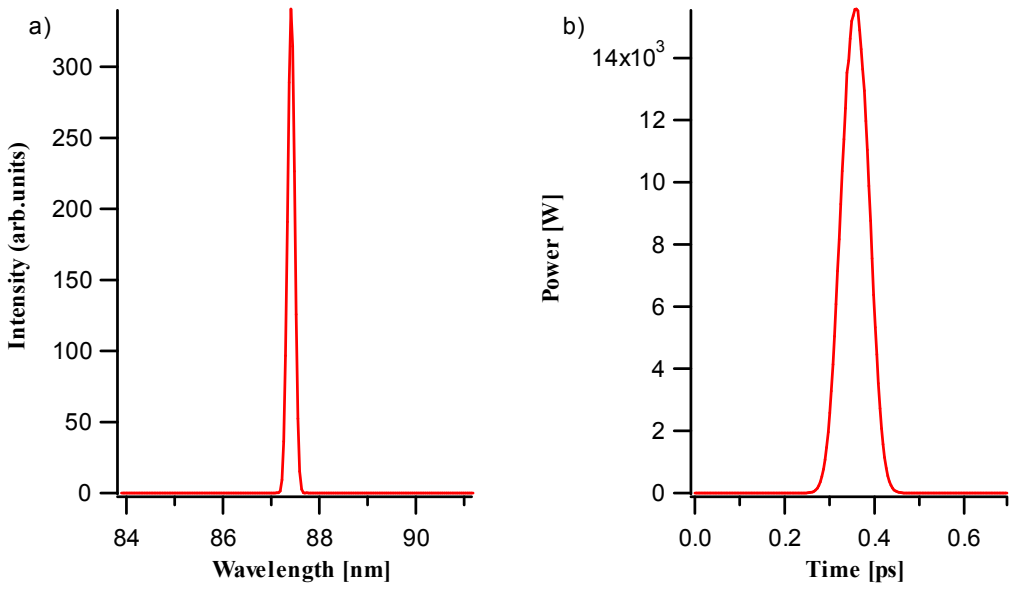

Figure 5.9: (a) Spectrum of the harmonic signal and (b) temporal profile of the harmonic signal.

5.2 SIMULATIONS OF CHG AT 195 nm

Here we report the simulations aimed at reproducing the results of the CHG experiment at 195 nm.

5.2.1 PRELIMINARY (TIME-INDEPENDENT) CALCULATIONS

The procedure was the same as in the preliminary calculations for the CHG at 87 nm. The purpose was to obtain the optimum value of the seed power, dispersive section strength and modulator and radiator wavelengths which maximize the radiation power.

The observed output power as a function of the input seed power (varying between 0 and 10 GW) is shown in Fig. 5.10. We observed a peak in output power around 3.4 GW of the seed power, after which the output decreases. Below 3.4 GW, the induced bunching is too small and, as a consequence, the output power is smaller than optimum. Above 3.4 GW, the seed power is too strong, the process reaches saturation too early and, as a consequence, the output power is reduced.

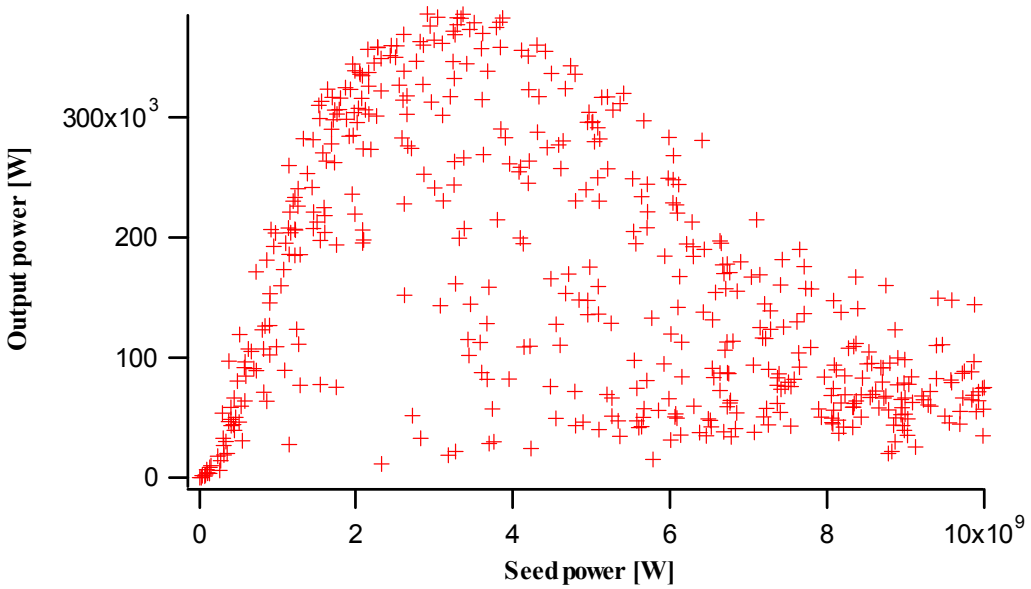

Figure 5.10: Output power at 195 nm as a function of the seed power at 0.75 GeV.

The dependence of the output power on the dispersive section strength is reported in Fig. 5.11. We see a peak in the graph very close to zero. This means that even with the magnetic field of the dispersive section set close to zero we can produce a satisfactory micro-bunching inside the modulator.

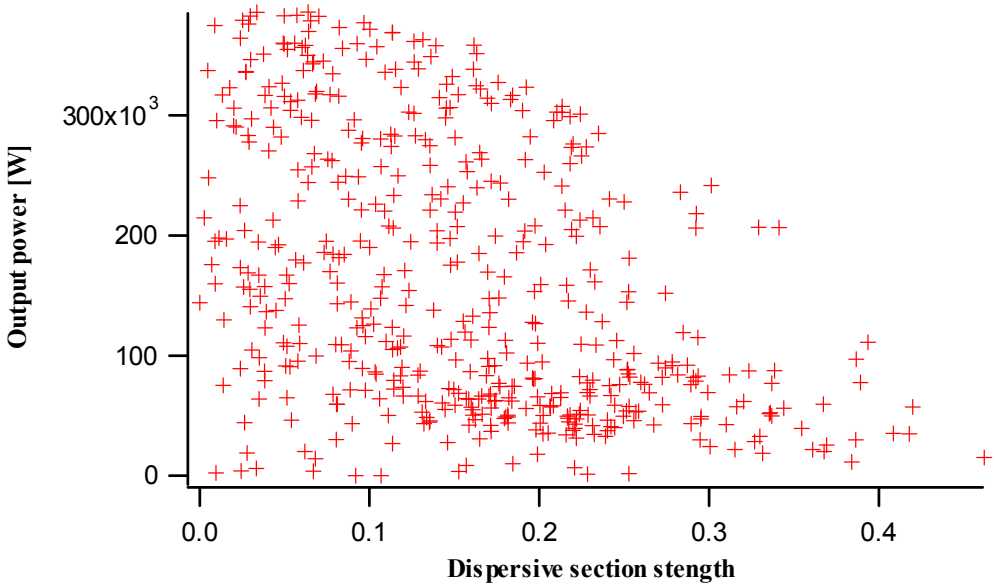

Figure 5.11: Second harmonic power as a function of the dispersive section strength (in "GENESIS" units).

For our simulations, we tuned the modulator at the same wavelength as the seed laser (390

nm) and the radiator at the second harmonic (195 nm). Fig. 5.12 shows the output power as a function of the variation of the modulator wavelength.

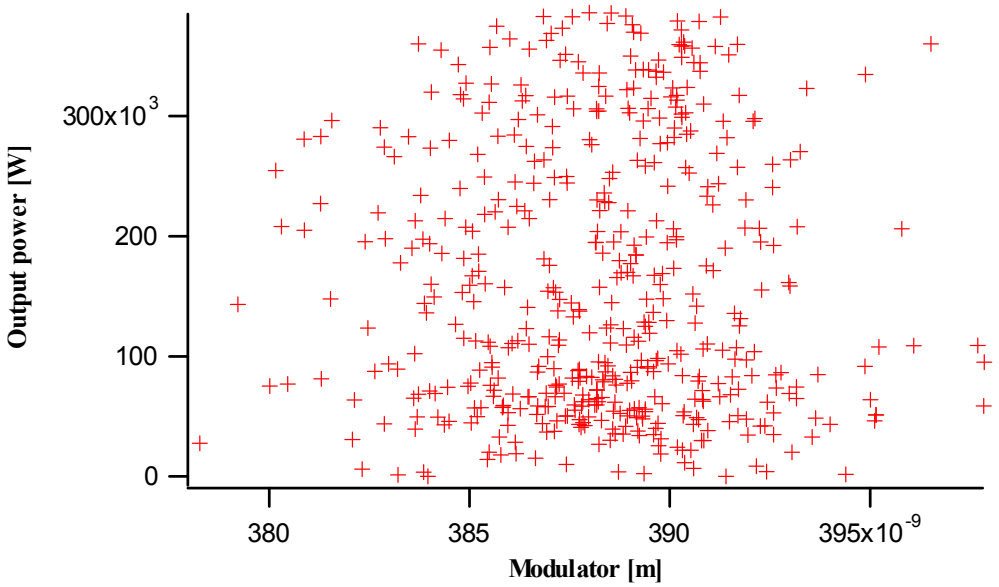

Figure 5.12: The output power as a function of the tuned wavelength of the modulator.

The performance of the output power at different wavelength of the radiator is shown in Fig. 5.13.

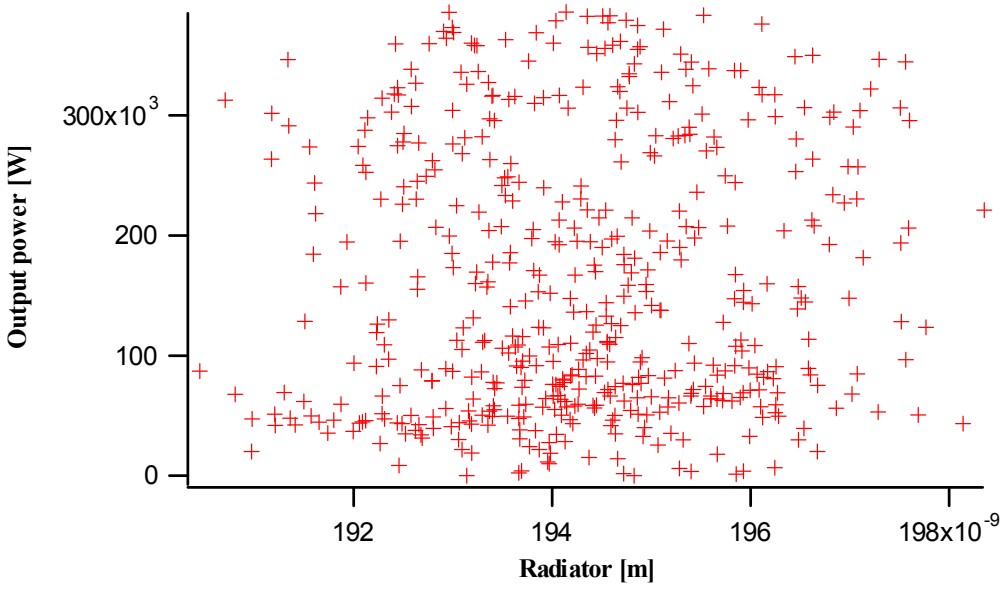

Figure 5.13: The output power as a function of the tuned wavelength of the radiator.

5.2.2 EXPECTED PERFORMANCE: TIME-INDEPENDET MODE

We performed simulations in time-independent mode using the optimum values obtained from the preliminary calculations reported in the previous Section. Those values are shown in Table 5.3.

Table 5.3: Main parameters used to find the optimal output power. For the reported simulations, the electron-beam energy is fixed at 0.75 GeV and the peak current is 10 A.

Seed Power (GW)	3.29
Modulator Wavelength (nm)	386.84
Radiator Wavelength (nm)	194.58
Dispersive Section Strength (mm)	0.49

Fig. 5.14 shows the evolution of the bunching along the radiator. We see a peak in the curve, which means that the bunching reaches saturation.

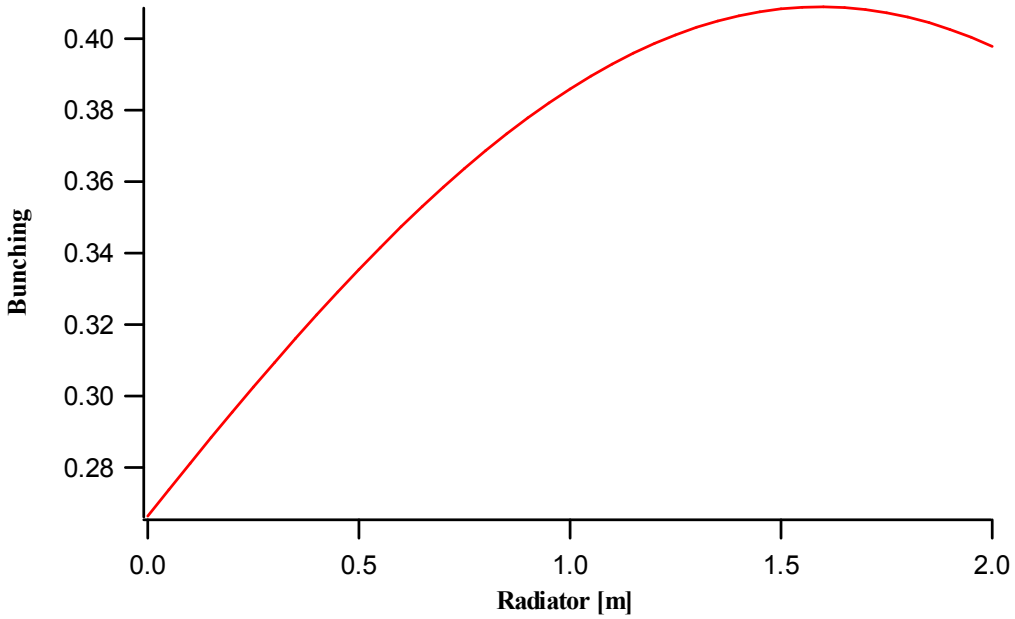

Figure 5.14: Evolution of the bunching along the along the radiator.

Third harmonic output power along the radiator is shown in Fig. 5.15. As in the case at 87 nm, the radiator length is not enough to reach the power saturation.

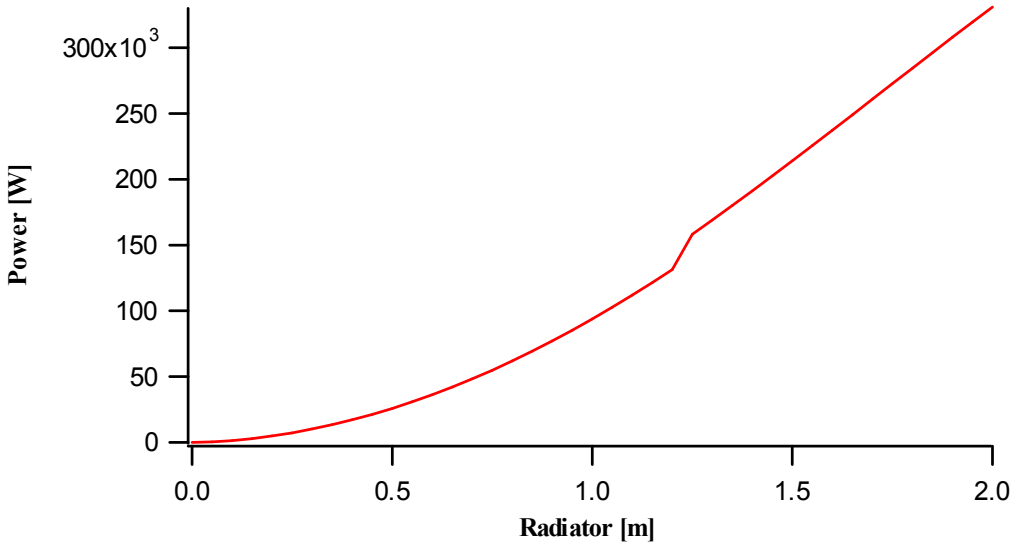

Figure 5.15: Output power along the radiator at 195 nm.

5.2.3 EXPECTED PERFORMANCE: TIME-DEPENDENT MODE

In Fig. 5.16a we report the spectrum of the second harmonic signal at the radiator exit. The temporal profile of the harmonic signal is shown in Fig. 5.16b. We see that the output power is about 380 kW. Analyzing the spectral profile we calculated the number of photons in one harmonic pulse at 195 nm. The number is 4.3×10^{10}. This will later be used in a comparison with the experimental result. The peak current is 10 A and the bunch duration is 30 ps.

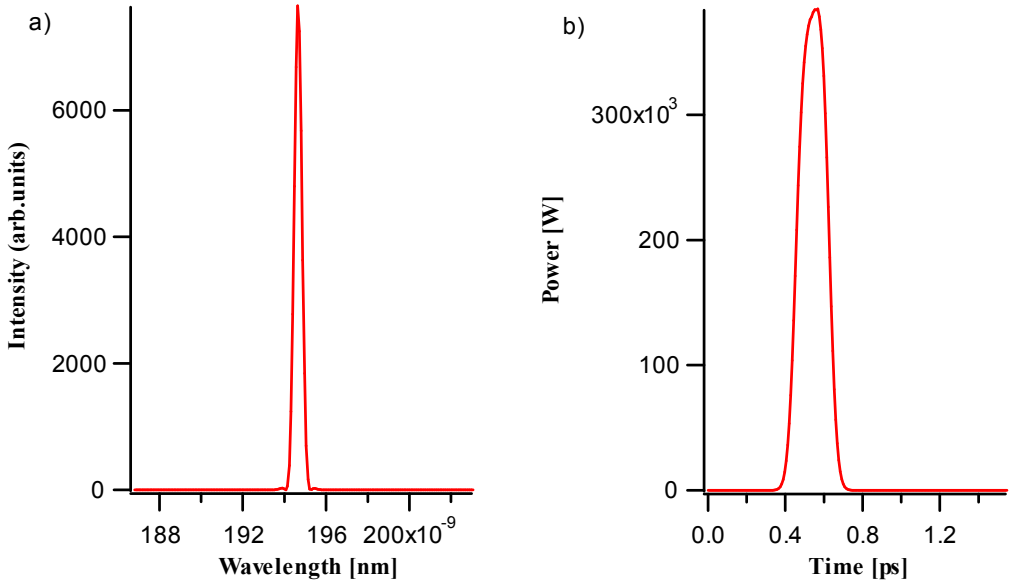

Figure 5.16: (a) Spectrum of the harmonic signal and (b) temporal profile of the harmonic signal.

6 CONCLUSIONS

In this chapter we compare the experimental results with simulations, conclude and give the perspectives of this facility.

6.1 COMPARISON: SIMULATION VS. EXPERIMENT

In Table 6.1 we present the comparison between the number of photons per pulse in simulations and experiments.

Table 6.1: Comparison experiments vs. simulations.

	Number of photons per CHG pulse
87 nm	
Experiment	3.3×10^{7}
Simulation	5.2×10^{8}
195 nm	
Experiment	2.4×10^{9}
Simulation	4.3×10^{10}

For both wavelengths, simulations overestimate the experimental result by approximately a factor 10. This discrepancy can be in part attributed to the fact that simulations assume a perfect spatial and temporal overlap between the seed pulse and the electron bunch inside the modulator, while such conditions are normally only partially met in experiments.

6.2 PERSPECTIVES

Harmonic Generation using Free-Electron Laser is motivated by the fundamental need of generating good quality radiation in the VUV/X-ray spectral region, beyond the reach of conventional light sources. Good quality means high flux, spatial and temporal coherence, adjustable duration (great interest mainly to short – fs – pulses) and good stability. Achieving

this challenging goal will provide the opportunity to open the path to more detailed investigations of many new areas of science, such as nanotechnology.

We have demonstrated that the Elettra FEL is a coherent source able to provide ultra-short and stable radiation down to 87 nm. This makes the Elettra FEL a presently unique source. The number of photons per FEL pulse at this wavelength (about $\sim 10^7$) and the relatively high peak power (0.7 kW) make this source a promising tool for the investigation of dynamical phenomena with sub-ps time resolution. With the help of simulations, we were able to study the dependence of optimum performance from the main (adjustable) experimental parameters.

This work provides experimental results supporting the idea of FELs as a new generation of light sources. We have demonstrated that seeded coherent harmonic generation on electron storage rings can significantly extend the potential of the presently available light sources, allowing new investigations in the realm of both basic and applied research fields.

Bibliography

[1] DELSY, http://wwwinfo.jinr.ru/delsy/Home_delsy.htm

[2] Robinson A. L., http://xdb.lbl.gov/Section2/Sec_2-2.html

[3] Shintake T., *Proceeding of PAC07*, Albuquerque, New Mexico, USA (2007)

[4] LEUTL, http://www.aps.anl.gov/aod/mcrops/leutl/

[5] VISA, http://www-ssrl.slac.stanford.edu/visa/talks/visa_080901_tremaine.pdf

[6] TTF,http://zms.desy.de/research/photon_science/free_electron_laser_flash/index_eng.html

[7] SCSS, http://www-xfel.spring8.or.jp/fist_lasing/FirstLasingofSCSS.html

[8] LCLS, http://lcls.slac.stanford.edu/

[9] Wang X.J. *et. al., Proceeding of FEL 2006,* BESSY, Berlin, Germany

[10] The Conceptual Design Report of the FERMI@Elettra Project, Trieste, Italy (2007)

[11] Curbis F., *Generation of VUV ultra-short coherent optical pulses using electron storage rings*, Universita degli Studi di Trieste, Trieste, Italy (2008)

[12] Renieri A., *Proceeding of the 27th International Free Electron Laser Conference*, Stanford, California, USA

[13] Girard B. *et. al., Phys. Rev. Lett*. **53**, 2405 (1984)

[14] Labat M. *et al., Eur. Phys. J. D* **44**, 187 (2007)

[15] De Ninno G., *Introduzione alla fisica degli Acceleratori*, Lecture Notes, Universita degli Studi di Trieste, Trieste, Italy (2006)

[16] De Ninno G., *Introduzione alla fisica dei Laser a Elettroni Liberi*, Lecture Notes, Universita degli Studi di Trieste, Trieste, Italy (2004)

[17] ELETTRA FEL Parameter List,
http://www.elettra.trieste.it/projects/euprog/fel/FEL_parameters.html

[18] Coherent, www.coherent.com

[19] sub-ps laser timing stabilization, www.tbwp.com

[20] Ferianis M., "The Elettra Streak Camera: system set-up and first results", *Proc. of the DIPAC 1999 Conf.,* Chester, UK (1999)

[21] Tanaka Takashi and Kitamura Hideo, http://radiant.harima.riken.go.jp/spectra/

[22] Reiche Sven, http://corona.physics.ucla.edu/~reiche/

Other related papers:

[23] Bonifacio R., L. De Salvo Souza and Pierini P., *Nucl. Inst. and Meth. A* **296** 787 (1990)

[24] De Ninno G. *et. al., Nucl. Instrum. Methods Phys. Res. A* **507** 274 (2003)

[25] Ferianis M., *et al., Proceeding of FEL 2004*, 2004.

[26] Freund H.P. and Antonsen T.M., *Principles of Free-electron Lasers*, Chapman & Hall, London, UK (1992)

[27] Rodwell M. J. W., *et al., IEEE J. Quantum Electron.* **25** 817 (1989)

[28] Van der Geer C. A. J., *FELIX Design and Instrumentation*, Technische Universiteit Eindhoven, Eindhoven, Netherlands (1999)

[29] Spezzani C *et. al., Nucl. Instrum. Methods Phys. Res. A* **596** 451 (2008)

[30] Yu L.H. *et. al., Phys. Rev. A* **44** 51178 (1991)

[31] Yu L.H. *et. al., Phys. Rev. Lett.* **91** 7 (2003)

APPENDIX A

Table A.1: A description of the input parameters for GENESIS simulations.

Parameter	Description	Unit
AW0	The normalized, dimensionless rms undulator parameter.	unitless
XLAMD	The undulator period length	meter
GAMMA0	The RMS value of the energy distribution in terms of electron rest mass energy	unitless
DELGAM	The RMS value of the energy distribution in terms of electron rest mass energy	unitless
RXBEAM	The rms value in x of the transverse, spatial distribution	meter
RYBEAM	The rms value in y of the transverse, spatial distribution	meter
EMITX	The normalized rms emittance in x	meter
EMITY	The normalized rms emittance in y.	meter
ALPHAX	Rotation of the transverse phase space distribution in x according to the standard definition $ALPHAX = \frac{< xx' > GAMMA}{EMITX}$.	unitless
ALPHAY	Rotation of the transverse phase space distribution in y according to the standard definition $ALPHAY = \frac{< xx' > GAMMA}{EMITY}$.	unitless
XLAMDS	The resonant radiation wavelength.	meter
PRAD0	The input power of the radiation field.	Watt
NWIG	The number of periods within a single undulator module.	unitless
CURPEAK	Peak current of the electron beam. Time-independent simulations enforces a constant current.	Amperes
IBFIELD	Magnetic field of the dispersive section	Tesla

APPENDIX B

THE INPUT FILES FOR GENESIS USED IN SECTION 5.1.2.

MODULATOR

AW0 = 3.9579
XLAMD = 1.000000E-01
GAMMA0= 1.783E+03
DELGAM= 2.139E+00
RXBEAM= 1.1225E-04
RYBEAM= 3.5496E-05
ALPHAX= 0.24E+00
ALPHAY= 0.89E+00
EMITX = 2.46E-06
EMITY = 2.46E-07
XLAMDS= 2.6134863e-007 ,
PRAD0= 1.4890212e+009 ,
NWIG = 20
CURPEAK= 76.69E+00

RADIATOR

AW0 = 2.1341
XLAMD = 1.000000E-01
GAMMA0= 1.783E+03
DELGAM= 2.139E+00
RXBEAM= 1.1225E-04
RYBEAM= 3.5496E-05
ALPHAX= 0.24E+00
ALPHAY= 0.89E+00
EMITX = 2.46E-06
EMITY = 2.46E-07
XLAMDS= 8.7667632e-008 ,
PRAD0 = 2.500000E-09
NWIG = 20
CURPEAK= 76.69E+00
IBFIELD= 3.4541957e-001 ,